

Contents lists available at ScienceDirect

Chemical Engineering Journal

journal homepage: www.elsevier.com/locate/cej





Passivation of iodine vacancies of perovskite films by reducing iodine to triiodide anions for high-performance photovoltaics

Yifang Qi^a, Kevin A. Green^b, Guorong Ma^b, Surabhi Jha^b, Kristine Gollinger^a, Chen Wang^c, Xiaodan Gu^b, Derek Patton^b, Sarah E. Morgan^b, Qilin Dai^{a,*}

- ^a Department of Chemistry, Physics, and Atmospheric Sciences, Jackson State University, Jackson, MS 39217, United States
- b School of Polymer Science and Engineering, Center for Optoelectronic Materials and Devices, The University of Southern Mississippi, Hattiesburg, MS 39406, United States
- ^c Department of Chemistry and Biochemistry, Queens College, City University of New York, Flushing, NY 11367, United States

ARTICLE INFO

Keywords: Inverted perovskite solar cells Tetrabutylammonium chloride Passivation Stability

ABSTRACT

Inverted perovskite solar cells (PSCs) exhibit great potential in large-scale fabrication due to the low-temperature manufacturing process and low cost compared to normal PSCs. However, defects at the surface and grain boundaries (GBs) of perovskite films, such as iodine vacancies, lead to low efficiency and poor stability. Herein, we report a strategy to passivate the defects in situ with tetrabutylammonium chloride (TABCl). Both the surface defects and GB defects are passivated after perovskite film growth. Moreover, TABCl modifies iodine vacancies by reducing $\rm I_2$ to iodide ions, leading to a decrease in charge recombination in the films and enhanced device performance. The power conversion efficiency (PCE) of devices increases from 18.52% to 20.36 % by TBACl modification, and TBACl also reduces the Voc loss in the PSCs. Meanwhile, TBACl enhances the UV light stability of devices tested by continuous UV light irradiation due to the decreased defects by TBACl. The PSCs could maintain over 90% PCE under continuous UV light irradiation for 450 min. This work not only presents a method to effectively passivate the defects in situ including the surface defects and GB defects but also demonstrates a novel strategy to modify the iodine vacancies by the reducibility of TBACl. In addition, the reducibility of TBACl suppresses the degradation of perovskite films, leading to improved stability.

1. Introduction

In the past decade, hybrid organic–inorganic PSCs have drawn much attention, and the power conversion efficiency (PCE) has reached 25.7% [1]. Inverted structure (p-i-n) PSCs are lightweight and enable low-cost, low-temperature manufacturing compared to the normal structure (n-i-p) PSCs, thus they have the great potential for large-scale fabrication [2,3]. However, the highest PCE of inverted devices is 22.7%, which is still lower than the devices with normal structure [4]. The trap states influence the PCE of devices significantly, which are always located at the surface and grain boundaries (GBs) of perovskite films due to the solution-processed fabrication method [5-7]. Besides, Γ can be oxidized into Γ (iodine) and volatilized during the perovskite film annealing. Therefore, iodine vacancies are one of the major defects in perovskite films [8,9]. In addition, the hysteresis effect and the device degradation are also attributed to GBs due to the ion migration pathways [10]. Moreover, GBs are also frail to moisture, leading to poor stability of the

PSCs. It is believed that significant potential to improve the performance of PSCs is achievable by passivating the surface and GBs defects [11,12]. Therefore, the investigation of the surface and GBs passivation is very necessary to the development of PSCs toward high efficiency and high stability.

Significant progress has been made through defect passivation of PSCs [13-15]. Bian *et al.* used polymeric interlayer to achieve formamidinium lead tri-iodide perovskite films with reduced defects and high-efficiency devices [16]. They also employed the 4-fluoro-phenethy-lammonium iodide and poly (9-vinylcarbazole) (PVK) to modulate the growth of the FAPbI₃ films to obtain high-efficiency devices [17]. Zheng *et al.* used three mercaptobenzimidazole-based molecules to passivate the defects between the perovskite and electron transport layer (ETL) layer and enhanced the PCE from 19.5% to 21.2% [18]. Luo *et al.* improved the PCE from 15.9% to 18.2%, using 1-methyl-3-propylimidazolium bromide (MPIB) [19]. Methylammonium iodide (MAI) was reported to passivate the GBs defects to enhance the device performance

E-mail address: qilin.dai@jsums.edu (Q. Dai).

^{*} Corresponding author.

[20]. The surface defects can be passivated by tetrapropylammonium iodide through strong ionic interactions [21]. Wang et al. utilized trimethylammonium chloride to passivate the GBs defects [22]. Cheng et al. studied the surface defect passivation by cysteamine hydrochloride PSCs [23]. Qi et al. used pentaerythritol tetrakis(3mercaptopropionate) to decrease the uncoordinated Pb2+ defects in the perovskite films and thus increased PCE of the devices from 19.0% to 21.4% [24]. Wei et al. added tetrabutylammonium bromide into perovskite precursor solution to modify the defects of perovskite films to increase the device performance [25]. However, the tetrabutylammonium bromide in the perovskite solution affects the perovskite growth environment. Therefore, the increased device performance may be also related to the perovskite growth. It is hard to illustrate the effects of the defects on the device efficiency. However, the reported passivation methods introduce the passivants either in the perovskite precursor solution or in an anti-solvent drop-casting process to modify the perovskite film defects. The defect passivation and perovskite film growth occur simultaneously. Therefore, the perovskite films grow in the presence of passivants, leading to the modified perovskite film growth process. It is a challenge to evaluate the defect passivation effect on the device performance since the improved device performance is also attributed to the modified perovskite film growth process. It is pivotal to develop a method to estimate the defect passivation effect on the PSC performance without affecting the perovskite film growth to fundamentally understand how much room remains to improve the PSC performance via defect passivation strategy.

Iodine vacancies in perovskite films are formed because of the loss of iodide ions by the volatilization of MAI during the perovskite film annealing process [26-29]. In addition, perovskite films slowly decompose, leading to the production of I2 and iodine vacancies [30-32], which is the unstable nature of the iodine compounds. Huang et al. reported that I2 is always produced as a side product in the perovskite films due to the fabrication process of the films [33], and I2 is not stable due to fast volatilization [26-29]. Therefore, I2 is formed in the perovskite films, and is fast volatilized, leading to the production of iodine vacancies. Additional iodine vacancies are produced with the time of aging due to the properties of iodine compounds [33]. Iodine vacancies play a role as defects and are detrimental to the device performance. Ren et al. introduced formamidinium bromide to reduce traps by iodine vacancy filling because bromine can eliminate uncoordinated Pb⁰ [34]. Wu et al. added the pyridinium iodide to passivate defects in perovskite films by filling negatively charged iodine vacancies and interacting with positive defects, enhancing the PCE from 20.37% to 21.42% [35]. Haque et al. utilized phenylethylammonium iodide to passivate the iodine vacancies and tackled morphological imperfections of perovskite films [36]. Xu et al. studied fluorinated organic halide salt 4-fluorophenethylammonium iodide to passivate the iodine vacancies in the perovskite films and enhance the PCE of the PSCs from 19.5% to 21% [37]. However, it seems that the reported methods can not suppress the production of iodine vacancies since research efforts have been focused on filling the iodine vacancies by the external iodide source. Furthermore, the films keep generating new iodine vacancies even if the old iodine vacancies are filled, which may be the real reason for the poor long-term stability of PSCs. It is anticipated that suppressing the generation of iodine vacancies in perovskite films will enhance the long-term stability of PSCs. Xie et al. introduced tetrabutylammonium iodide to modify defects in perovskite solar cells [36]. However, we report that the TBACl can reduce I₂ to I₃, leading to the reduced defects of the perovskite films and improved device stability, which provides a new strategy to achieve high-performance devices. Moreover, we systemically study the device and film stability by different light sources under different conditions, and our device stability is much better than theirs. In addition, we also systemically study the origins of the improved device performance in terms of charge transport (ultrafast spectroscopy, and steady-state PL), and charge recombination (LED devices). Therefore, our work provides significant fundamental science to the field, which opens a new door to

achieve high efficiency and high stability devices.

Poor stability of PSCs under light exposure conditions, especially UV light is another factor that limits the practical applications of PSCs. It is well known that I2 is generated under exposure to UV light which induces iodine vacancies in the perovskite films layer, leading to poor stability [38]. Nishino et al. inserted Sb₂S₃ as a blocking layer between ETL and perovskite layer to improve the light stability of devices [39]. Deng et al. increased the UV light stability of devices by inserting a polymer layer to block UV light, and their devices maintained the initial PCE after ~ 700 h under UV light irradiation [40]. Bella et al. developed fluorinated photopolymer coatings on the PSCs to protect the devices from degradation under UV light [41]. Dai et al. enhanced the stability of the PSCs under UV light irradiation using NH₄I as an interfacial modifier between the electron transport layer and perovskite layer and the devices maintained 70% of the original PCE for over 20 h under UV light stress tests [42]. Kang et al. enhanced the UV-light stability of PSCs using an SrO interlayer to protect perovskite layer degradation [43]. Although the blocking layer could enhance the light stability of the devices, the blocking layer may influence the carrier transport and cause a decreased current. Furthermore, the blocking layer method cannot stop the perovskite film decomposition. Therefore, it is necessary to find new ways to improve the light stability by suppressing the perovskite film decomposition, which may solve the UV light stability problem.

In this work, we report TBACl as a low-cost material to passivate the perovskite films in situ an approach that does not affect the perovskite film growth process. The passivation treatment is carried out after perovskite film growth. Both the surface and GBs defects are effectively modified. Furthermore, TBACl can reduce I2 to I3 due to the reducibility to suppress the I2 generation and decrease the number of iodine vacancies in the perovskite films, leading to iodine vacancy modification. Moreover, TBACl passivation improves the light stability of PSCs, especially UV light irradiation, since the perovskite film decomposition is suppressed by TBACl. In addition, TBACl can suppress I2 releasement from perovskite films and slow the degradation of perovskite films, leading to improved aging stability. Benefiting from the TBACl passivation, the PCE of devices increase from 18.52% to 20.36 %. The TBACl modified devices keep \sim 90% of the initial PCE under continuous UV light irradiation for 450 min. In contrast, the control device only could maintain $\sim 51\%$ of the initial PCE value under the same UV light soaking conditions. Thus, we present a low-cost, facile, and effective in situ strategy to enhance the performance of the device comprehensively.

2. Experimental section

2.1. Materials

N, N-Dimethylformamide (DMF, Anhydrous 99.8%), Isopropanol (IPA, Anhydrous 99.5%), chlorobenzene (CB, Anhydrous 99.8%) and Methylammonium iodide (MAI) were purchased from Sigma-Aldrich (USA). [6,6]-phenyl C_{61} -butyric acid methyl ester (P C_{61} BM) was received from Nano-C Crop (USA). Lead iodide (PbI $_2$, 99.98%), Silver (Ag, 99.99%), Bathocuproine (BCP) and Dimethyl sulfoxide (DMSO, 99.8%) were purchased from Alfa Aesar (USA). Poly[bis(4-phenyl) (2,4,6-trimethylphenyl) amine] (PTAA, greater than99%) with molecular weight of 10 kDa was obtained from Solaris Chem (Canada). Tetrabutylammonium chloride (TBACl) was purchased from Tokyo Chemical Industry (Japan). ITO coated glass substrates (~9 Ω /sq) were received from Advanced Election Technology Co., Ltd (China). All chemicals were used as received.

2.2. Device fabrication

Patterned ITO coated glass substrates were cleaned by detergent, water, acetone, deionized water, and isopropanol sequentially by an ultrasonic bath for 15 min each. The glass substrates were treated by UVO for 30 min followed by drying with N_2 . After that, the glass

substrates were moved into a nitrogen glovebox ($O_2 < 0.1$ ppm and H_2O < 0.1 ppm). Firstly, the PTAA solution (3 mg/mL in CB) was spin-coated on the ITO substrates at 4000 rpm for 30 s, and the films were annealed at 100 °C for 10 min. The perovskite precursor solution (PbI₂, 1.2 M, and MAI 0.3 M in mixed solvents of 1 mL DMF and 85 µL DMSO) was spincoated on the ITO/PTAA at 6000 rpm for 20 s, then the MAI solution (30 mg/mL in IPA) was dropped on the top of the film with 4000 rpm for 40 s. After annealing the films at 100 °C for 30 min, TBACl in IPA with different concentrations were spin-coated on the perovskite film at 4000 rpm for 30 s. Then the wet films were annealed at 70 $^{\circ}\text{C}$ for 10 min. PC₆₁BM solution (20 mg/mL in CB) was spin-coated on the film with 3000 rpm for 30 s followed by annealing at 90 $^{\circ}$ C for 30 min. Afterward, BCP solution (0.5 mg/mL in IPA) was spin-coated on the PC₆₁BM film at 4000 rpm for 30 s. Finally, the silver electrode (Ag) was evaporated on the top of the film under the vacuum of 6×10^{-4} Pa to obtain PSCs with the structure of ITO/PTAA/Perovskite/TBACl/PC61BM/BCP/Ag. The area of each device is 0.04 cm² which is defined by the shadow mask.

2.3. Characterization

The surface potential of the films was obtained by Kelvin probe force microscopy in Surface Potential mode and the morphology was obtained in tapping mode (Bruker Dimension Icon Atomic Force Microscope). The morphology of the films was also studied by using a field emission scanning electron microscope (LYR3 XMH, Tescan). The XRD diffraction peaks were obtained by MiniFlex600 (Rigaku) with Cu Ka radiation source $\lambda = 1.54056$ Å. The phase and crystallinity of perovskite were also collected by the Grazing-incidence wide-angle X-ray scattering (GIWAXS) based on a laboratory beamline system (Xenocs Inc. Xeuss 2.0) with an X-ray wavelength of 1.54 Å and incidence angle of 0.2° under vacuum condition. The images of GIWAXS were recorded on a Pilatus 1 M detector (Dectris Inc.) and processed using Irena and Nika package in Igor software. The UV-vis absorption spectra of perovskite films were taken by Cary 60 spectrophotometer (Agilent Technologies). The current density voltage (J-V) curves, as well as stabilized power output at the maximum power point, were obtained by digital source meter (Keithley, 2400, USA) under the illumination AM1.5G (100 mW/ cm²) with a G2V Pico solar simulator. The steady-state photoluminescence (PL) spectra and the time-resolved photoluminescence (TRPL) spectra of devices were collected by the fluorescence spectrometer (FluoroMax, Horiba) with DeltaHub and NanoLED. The excitation wavelength is 461 nm. The water contact angle measurement of the films was carried out using a contact angle goniometer (Ossila). The series and recombination resistance of devices were obtained by an electrochemical workstation (CHI 604E) with a 0.9 V bias. The monochromatic incident photon-to-electron conversion efficiency (IPCE) spectra of devices were collected by a quantum efficiency measurement system (IQE-200B, Newport). The dark J-V curves of electron-only and hole-only devices were measured by the source meter (Keithley, 2450, USA). XPS analysis was performed using a Thermo-Fisher ESCALAB Xi + spectrometer equipped with a monochromatic Al X-ray source (1486.6 eV, 300 mm² spot size). Measurements were performed using the standard magnetic lens mode and charge compensation. The base pressure in the analysis chamber during spectral acquisition was $3 \times 10^{-}$ mBar. Spectra were collected at a takeoff angle of 90° from the plane of the surface. The pass energy of the analyzer was set at 20 eV for highresolution spectra and 150 eV for survey scans, with energy resolutions of 0.1 eV and 1.0 eV, respectively. Binding energies were calibrated with respect to C 1 s at 285.3 eV. All spectra were recorded using the Thermo Scientific Avantage software data files were translated to VGD format and processed using the Thermo Avantage package v5.9904. UV light stability of the PSCs is performed by a BLAK-RAY Ultraviolet Lamp (365 nm, Model B 100 AP). The light intensity on the devices is similar to that of the standard sun (tested by Newport Power Meter Model 1930C and Newport model 918-SL). The light stability (without UV component) is carried via a 100 W incandescent light bulb (10 mW on the

devices). The transient absorption measurement system is described in the supporting information and Figure S1.

3. Results and discussions

TBACl is introduced to modify perovskite MAPbI3 films. The fabrication process of PSCs (with the inverted structure of ITO/PTAA/ MAPbI₃/TBACl/PC₆₁BM/BCP) modified by TBACl is shown in Fig. 1a. A typical two-step method is used to fabricate inverted PSCs. Perovskite film growth is terminated by annealing. Then, TBACl is spin-coated on the top of perovskite films to realize the in-situ passivation of the perovskite films. Surface defects of the perovskite films are passivated. In addition, the interface between perovskite film and PC₆₁BM is modified, which may facilitate the charge transport in the devices. Thermal annealing of the films ITO/PTAA/MAPbI₃/TBACl is leveraged to not only promote the interactions between MAPbI3 and TBACl but also hasten the TBACl solution to diffuse into the perovskite films to further modify the grain boundaries (GBs) of the films (Fig. 1b), which is also manifested by SEM EDX image (linear mode scan) of the device (ITO/PTAA/perovskite/TABCl/PC₆₁BM/BCP/Ag) in Figure S2. It can be seen that the intensity of Cl element varies along with the I element intensity across the device (Figure S2), indicating the existence of Cl in the device. The molecules of TBACl are smaller compared to the perovskite GBs, leading to effective diffusion and modification of the GBs. Most importantly, the reducibility of TBACl can reduce the iodine to iodide ions. Fig. 1c shows the photographs of I₂ in IPA solution and I₂ in IPA solution with TBACl. The color of I2 in IPA solution changes from orange to yellow as TBACl is added, indicating the decreased concentration of iodine in the solution. Fig. 1d shows the UV-vis absorption spectra of I2 in IPA solution, I2 in IPA solution with TBACl, and TBACl in IPA. The absorption spectrum of I2 in IPA solution shows a peak at 450 nm, which is consistent with the literature [44]. The absorption spectrum of I2 in IPA solution with TBACl exhibits an additional highintensity absorption peak at about 362 nm compared to I2 in IPA solution. Huang et al. reported that the absorption peak around 307 nm is assigned to the toluene-I2 complex [8]. However, they also attributed the 365 nm UV-vis absorption peak to I₃ in 2-ME solvent [45]. So, the UV-vis absorption peak may be related to the solvent. Seok reported UV-vis absorption peak of I₃ is located at 361 nm [44]. Therefore, we believe the 362 nm absorption peak is originated from I3-. Iodine vacancies in perovskite films are formed because of the loss of iodide ions due to the unstable nature of the iodine compounds and the annealing process during the fabrication of the devices, which is unavoidable [26,28]. The absorption peak at 450 nm is attributed to the I₂, which is consistent with the literature [44]. The additional peak at 362 nm appears as the TBACl is added, and the 362 nm peak is assigned to the I₃ [44]. Therefore, we think I₂ is reduced to I₃⁻ by TBACl. Moreover, TBACl is an ionic compound, and it contains TBA⁺ and Cl⁻ two parts. We try different compounds similar to TBACl to reduce I2 including TBAI, and TBABr (Figure S3). It can be observed that all the curves treated by TBACl, TBAI, and TBABr show very obvious absorption peaks at 362 nm, indicating that TBACl, TBAI, and TBABr can reduce I2 to I3. Therefore, it is reasonable to conclude that I₂ is reduced to I₃ by TBA⁺. The reduction chemical reaction is highly possible related to TBA+. The detailed chemical mechanism about the electron acceptor or donor is still a challenge for us to figure out. As stated above, the loss of iodide ions of the perovskite films during the fabrication process leads to the production of iodine vacancies. We consider that iodine vacancies serve as defects in the films that lead to decreased performance. It is reported that the additional I₃ ions could reduce the concentration of vacancies of iodine and the deep-level defects of the perovskite films [44,46]. Therefore, I₃ ions generated by TBACl can modify the defects (iodine vacancies) of the perovskite films. Therefore, I2 is reduced to I3 by TBACl in the solution. For comparison, the absorption spectrum of TBACl in IPA solution is also shown in Fig. 1d, which just excludes the absorption of TBACl at 362 nm in the spectra. I2 is produced in the

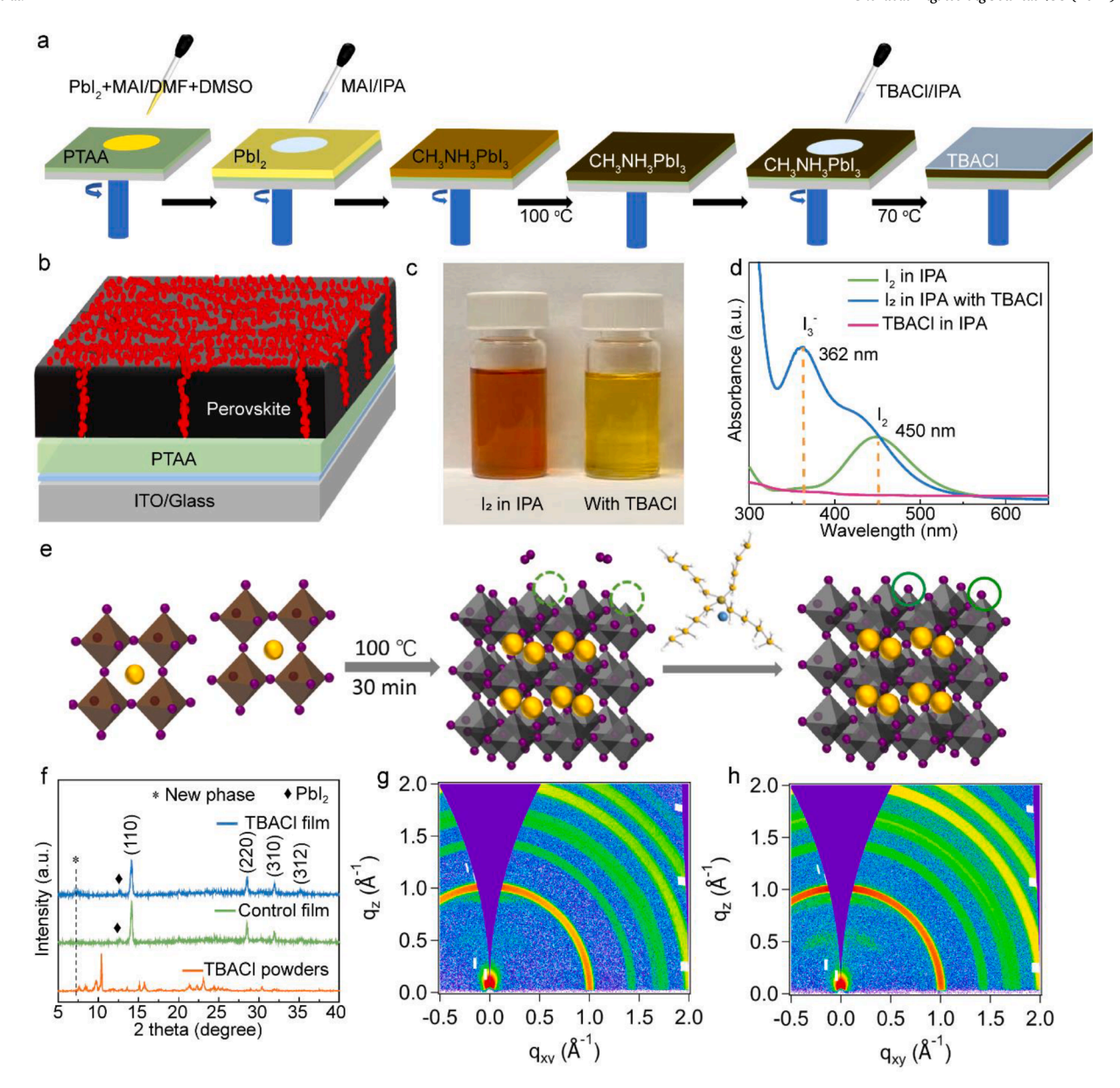


Fig. 1. a The fabrication process of perovskite films modified by TABCl; b The schematic of the perovskite film surface and GB passivation by TBACl; c the photograph of I_2 in IPA solution with and without TBACl; d the UV–vis absorption spectra of I_2 solution in IPA with and without TBACl; e The passivation schematic of perovskite film by TBACl; f The XRD diffraction patterns of perovskite film, perovskite with TBACl and TBACl powers; g and h The GIWAXS patterns of perovskite films without and with 0.05 mg/mL TBACl passivation.

perovskite films due to the fabrication process, then fast volatilized, leading to the production of iodine vacancies in the perovskite films [26-29]. TBACl can reduce I_2 in the perovskite films to I_3 , which modifies the iodine vacancies in the films. The schematic of iodine vacancies formation and modification by TBACl is shown in Fig. 1e. Iodine vacancies are formed during the film fabrication process due to the volatilization of MAI caused by the annealing. TBACl can passivate these iodine vacancies via the passivation effect. Moreover, I_2 is also produced slowly in the films and volatilizing after the film fabrication due to the film decomposition caused by the nature of iodine compounds. TBACl can reduce I_2 produced by the film decomposition to I_3 to passivate iodine vacancies, which suppresses film degradation, leading to improved device performance.

X-ray diffraction (XRD) patterns of TBACl powders, perovskite film without TBACl (control film), and perovskite film with TBACl (TBACl film) are shown in Fig. 1f. Both the control and TBACl films show XRD diffraction peaks at 14.14° , 28.52^{0} , and 31.94° , which are indexed into

(110), (220), and (310) crystal planes of perovskite films. The peaks at 12.66° are assigned to the (001) crystal planes of residual PbI2 in the control and TBACl films [47]. The residual PbI2 in the films doesn't affect the film performance according to the literature [48] An additional peak at 7.26° labeled by "*" is observed for the TBACl film, and this peak is not originated from TBACl compared to the XRD data of TBACl powers. This peak is also observed in the film prepared with PbI₂ with TBACl and cannot be observed in the film fabricated by MAI with TBACl (Figure S4). This peak is different from 2 dimensional (2D) perovskite peaks, which are at around 4° for n = 2 and 6° for n = 1 [49]. It doesn't show the additional PL peak before 700 nm (Figure S5), so the diffraction peak at 7.26° is not attributed to 2D perovskites. This indicates a new phase is produced by the TBACl modification via the reaction of TBACl and the Pb element. The full width at half maximum (FWHM) values of the (110) plane of control and TBACl films are 0.26° and 0.29°, respectively. TBACl doesn't influence the crystallinity of perovskite films, which is understood by the post-annealing process of TBACl after perovskite film growth. Fig. 1g and h show the 2D-GIWAXS images of control and TBACl films. Two main diffraction rings at q=1.0 and $2.0\ \text{Å}^{-1}$ are observed, which are assigned to the (110) and (220) planes of perovskite films [50]. Furthermore, a diffraction ring at $q=0.53\ \text{Å}^{-1}$ is observed, and the diffraction ring intensity increases with increasing TBACl concentrations (Figure S6). The diffraction ring at 0.53 Å^{-1} is attributed to the new phase, which is consistent with XRD results. The new phase may be related to the interactions between TBACl and perovskite films, leading to the stable contact between TBACl and perovskite for effective defect passivation, which is consistent with the results of XRD.

In addition, to study the influence of TBACl on the perovskite film morphology, control and TBACl films are characterized by SEM and AFM. Fig. 2a and b show the top-view SEM images of control and TBACl films, respectively. The grain sizes of 350 nm are obtained for the two films since the TBACl doesn't affect the perovskite growth process. Some pinholes are observed for the control film indicated by the red circles in Fig. 2a. Some particles are exhibited at the GBs for the TBACl film due to the TBACl modification (Fig. 2b), leading to reduced pinholes and surface defect passivation of the TBACl film. SEM cross-sectional images of the PSCs prepared by control and TBACl films are shown in Fig. 2c and d, respectively. A clear layer-by-layer structure is presented for both films. The thickness of the perovskite layer is about 250 nm. The TBACl film exhibits a much denser structure compared to the control film (Fig. 2d). This shows significant potential in facilitating the charge transport in the devices, resulting in high-efficiency devices [51,52]. Therefore, the TBACl passivation shows both surface and GB defect passivation. We also utilize AFM to investigate the roughness of the perovskite films affected by TBACl. Fig. 2e and f exhibit AFM topography images of the control and TBACl films, respectively. The rootmean-square roughness (RMS) values decrease from 17.6 nm to 15.3 nm as the perovskite film is modified by TBACl, so the perovskite film becomes smoother due to the surface modification by TBACl, leading to effective charge transport in the devices. Fig. 2g and h show the AFM phase images of control film and TBACl film, respectively. They look very similar to each other. In AFM images of the control and TBACl films (Fig. 2f and Fig. 2e), the roughness is improved by the TBACl, which could reduce charge recombination. In the TBACl film, the grain boundaries appear to be smoothed by the posttreatment with more regular features than the control film, which could reduce charge

recombination. The SEM and AFM results confirm the overall passivation effects of TBACl from the surface to the GBs.

Fig. 3a shows the contact potential differences (CPD) of the perovskite films with and without TBACl acquired through KPFM. The CPD of perovskite film is increased from -50 mV to 80 mV with TBACl modification and the variability is reduced. The increased CPD shows great potential in improving the carrier transport in the devices and enhancing V_{oc} of the devices [53,54]. To study the interaction between TBACl and perovskite films, FTIR spectra of the control and TBACl films are collected and shown in Fig. 3b and c. The NH_3^+ stretch of the TBACl film is located at $3176~\mathrm{cm}^{-1}$ compared to $3172~\mathrm{cm}^{-1}$ for the control film (Fig. 3b) [55]. The control film shows a peak located at 1578 cm⁻¹ (Fig. 3c), which is attributed to the stretching vibrations of N-H bond of perovskite film [56]. The peak shifts to 1576 cm⁻¹ as the perovskite film is modified by TBACl. The shift of the stretching vibration of NH₃⁺ and NH indicate the strong interactions between TBACl and perovskite films. According to the XPS results, it is possible that the interaction between perovskite films through NH₃⁺ and TBACl (N-H···Cl) (see XPS discussion). XPS measurements were carried out to further confirm the interactions between TBACl and perovskite film. The peak of C 1 s is collected to calibrate the spectra (Figure S7). As shown in Fig. 3d, The N 1 s peak corresponding to the ammonium groups in the control perovskite film appears at 401.7 eV, which shifts to lower binding energy at 401.3 eV after TBACl modification. Therefore, TBACl interacts with perovskite films, which is consistent with the FTIR results. N 1 s peak is attributed to N-H bonds, corresponding to the protonated amines (NH₃⁺) from the perovskite component of CH₃NH₃⁺. The shift of N 1 s may be attributed to the hydrogen bond between NH₃⁺ and TBACl in the perovskite (N-H···Cl) [57]. The control film exhibits two peaks at 142.8 and 138.0 eV, which are attributed to Pb $4f_{5/2}$ and Pb $4f_{7/2}$, respectively. The two peaks shift to 142.5 and 137.6 eV for the perovskite film treated with TBACl (Fig. 3e). Fig. 3f shows the XPS data of the I 3d. Two peaks attributed to I $3d_{3/2}$ and I $3d_{5/2}$ are located at 630.4 and 618.9 eV for the control film. However, the film treated with TBACl exhibits I $3d_{3/2}$ and I 3d_{5/2} peaks at 630.1 and 618.6 eV, respectively. The binding energy of Pb 4f and I 3d shift to lower energy is assigned to the interaction between uncoordinated Pb and TBACl [58-60]. The Pb-I bonding in the perovskite layer can be released by the coordination of Pb dangling bonds with TBACl, which is consistent with the shift of Pb 4f and I 3d peaks [58-60]. It is possible that the new phase observed in XRD results

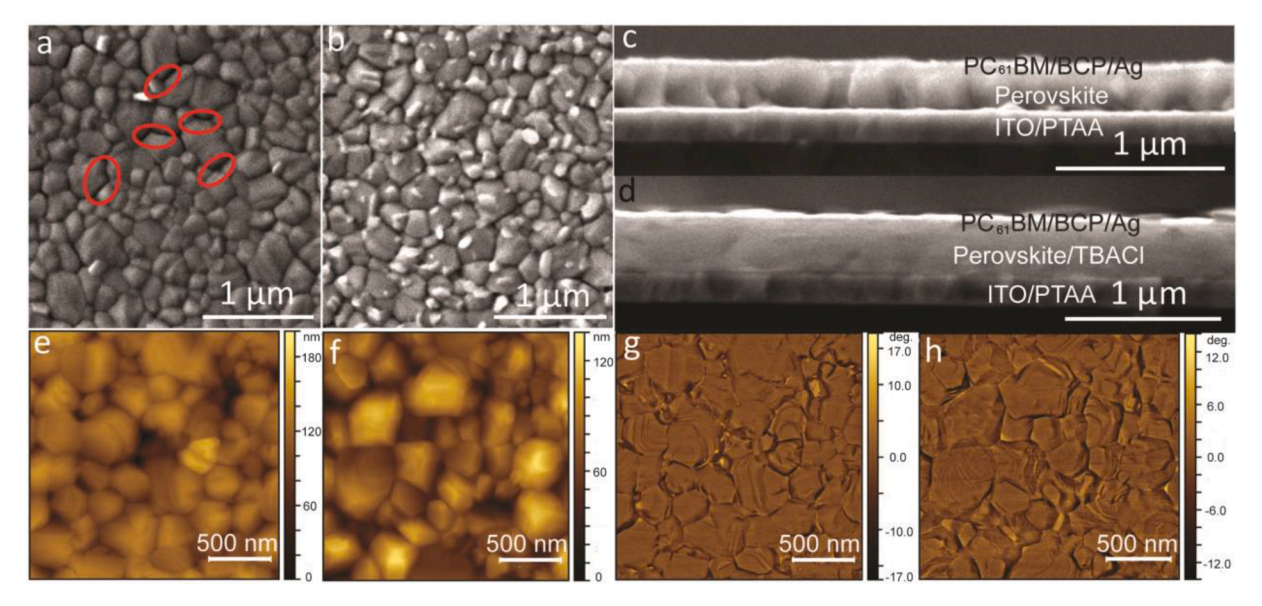


Fig. 2. a-b The top-view SEM images of perovskite films without and with TBACl passivation; c-d The SEM cross-section images of the PSCs without and with TBACl passivation; g-h The phase images of perovskite films without and with TBACl passivation.

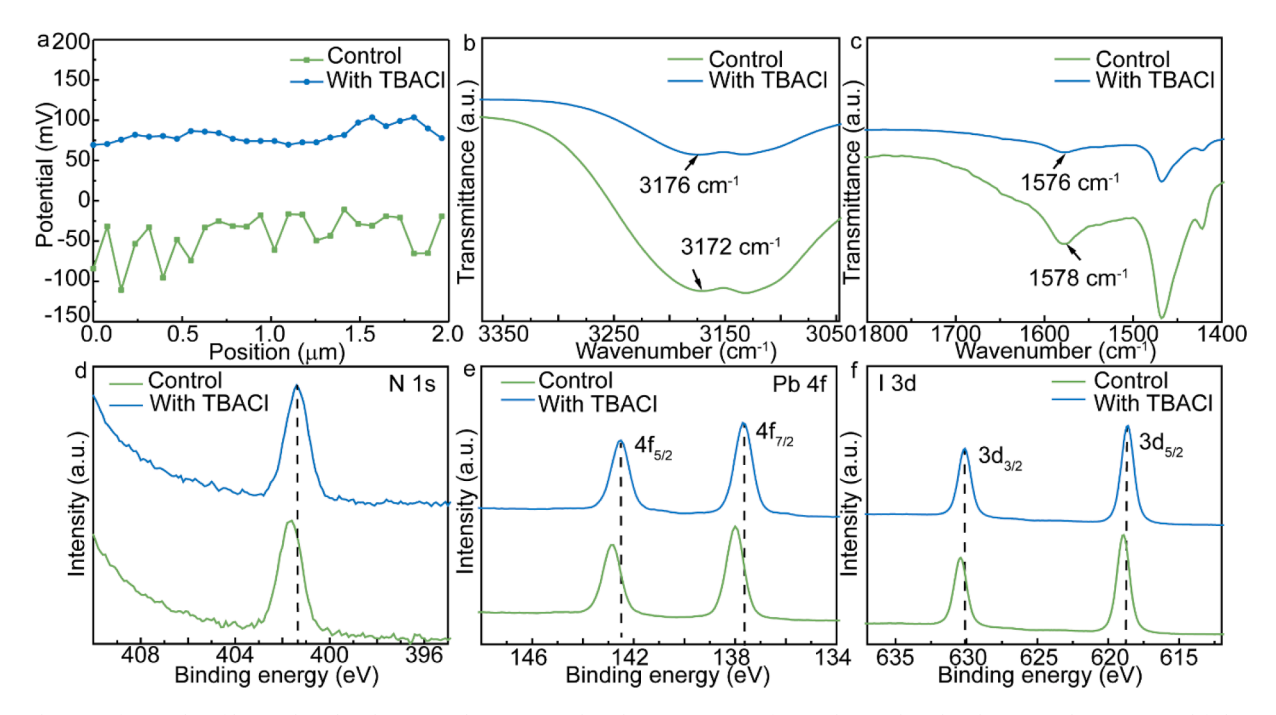


Fig. 3. a The CPD of perovskite films with and without TBACl passivation; b-c The FTIR spectra of perovskite with and without TBACl passivation; d-f The N1s, Pb 4f and I 3d XPS spectra of the perovskite films with and without TBACl passivation.

is associated with the shift of the XPS data. Therefore, FTIR and XPS results confirm the interactions between TBACl and perovskite films although TBACl is introduced after the perovskite growth. The interactions between TBACl and perovskite films attributed to the annealing process, leading to the interactions between the TBACl and perovskite films.

To assess the influence of TBACl modification on the efficiency of PSCs, current–voltage curves (J-V) of the devices are collected and the photovoltaic parameters are shown in Fig. 4a and Figure S8. The average PCE of devices increases from $\sim 18.7\%$ to $\sim 19.3\%$ as the TBACl

concentration increases from 0.01 mg/mL to 0.05 mg/mL. The average PCE of PSCs decreases to $\sim 16.5\%$ when the concentration of TBACl further increases to 0.1 mg/mL. Excess TBACl influences the electron transport from the perovskite layer to the PC₆₁BM, leading to inferior efficiency. Thus, the optimal TBACl concentration is 0.05 mg/mL. Fig. 4b shows the PCE distributions of control and the devices with TBACl (0.05 mg/mL) based on 35 devices for each experimental condition. The improved PCE of the TBACl devices is obvious compared to the control devices. In addition, the PCE of TBACl devices exhibits narrower distribution compared to that of the control devices, indicating

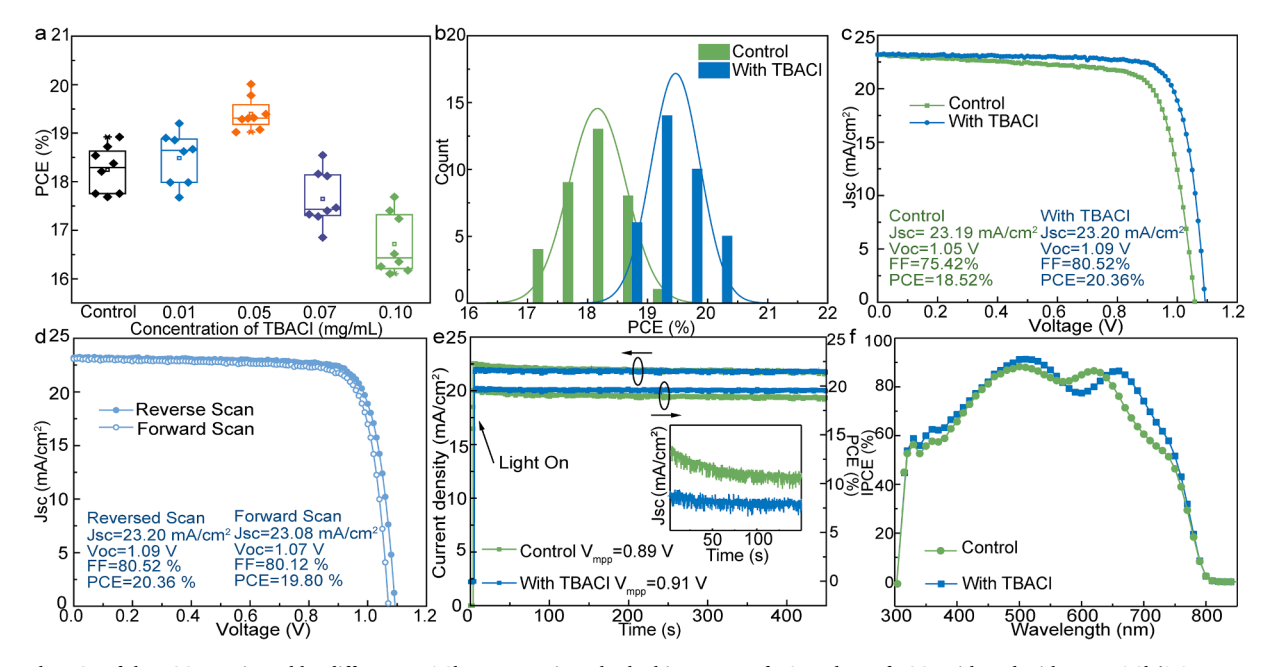


Fig. 4. a The PCE of the PSCs passivated by different TBACl concentrations; b The histograms of PCE values of PSCs with and without TBACl (0.05 mg/mL); c The champion devices with and without TBACl (0.05 mg/mL) passivation; d The hysteresis behavior of the PSCs with TBACl (0.05 mg/mL) passivation; e The steady-state current density and PCE output of the PSCs with and without TBACl (0.05 mg/mL). The inset shows the Jsc variation in the initial 150 s; f The IPCE spectra of the PSCs with and without TBACl (0.05 mg/mL) passivation.

the better reproducibility of the modified devices compared to the control devices. The optimized devices without and with TBACl (0.05 mg/mL) are displayed in Fig. 4c. The control device has a PCE of 18.52%with Jsc of 23.19 mA/cm², Voc of 1.05 V and FF of 75.42%, and the TBACl device shows the PCE of 20.36% with Jsc of 23.20 mA/cm², Voc of 1.09 V, and FF of 80.52%. The integral current density values of control and modified devices are 18.9 mA/cm² and 19.8 mA/cm², and the integrated current data are shown in Figure S9. So, the UV-vis absorption peak may be related to the solvent.. It is reported that the integrated current density of IPCE data is 10-20% less than the Jsc, which is acceptable, due to different light sources, ion migration, and degradation during the measurement by long-time light irradiation [61]. Significant improvement of Voc and FF is achieved by TBACl modification. The improved Voc is attributed to increased quasi-Fermi level splitting due to the decreased defect state density of the modified perovskite film caused by TBACl modification [62,63]. We obtain the highest occupied molecular orbital (HOMO) level of the perovskite by ultraviolet photoelectron spectroscopy (Figure S10 a and b). The HOMO level of the control and TBACl films are -5.43 eV and -5.4 eV. The bandgap of the perovskite is 1.5 eV [64]. Therefore, the LUMO level of the control and TBACl are 3.93 eV and 3.9 eV. The energy level structure diagram is shown in Figure S10 c. The energy levels of other layers are plotted according to the literature [65]. The origin of the Voc in PSCs is determined by the difference between the LUMO level of perovskite and the HOMO of PTAA [66]. Therefore, the device based on TBACl exhibits improved Voc. The increased FF of the modified device is ascribed to the reduced charge recombination because of the TBACl passivation. Fig. 4d shows the hysteresis effect of PSCs modified by TBACl, and the hysteresis index (HI) can be calculated by the following equation (1)[67],.

$$HI = \frac{PCE(reverse) - PCE(forward)}{PCE(reverse)} \tag{1}$$

where PCE (reverse) is the PCE value obtained by the reverse scan, and PCE (forward) is the PCE value obtained by the forward scan. The PCE values of the champion TBACl PSCs are 20.36 % and 19.80% for the reverse and forward scan, respectively. So, the HI of the modified device is calculated to be 1.05%, which is neglectable. The interfacial ion migration and the carrier trapping by the interfacial defects are the two main reasons for the hysteresis of devices according to previous reports [68-70]. Thus, we attribute the neglectable hysteresis effect of the modified devices to fewer surface and GB defects and the reduced ion migration in the devices due to TBACl passivation. To further confirm the TBACl effect on the device performance, the steady-state J_{sc} and PCE output of the PSCs with and without TBACl at the maximum output power point (0.91 V for TBACl device and 0.89 V for control device) are studied (Fig. 4e). The steady-state J_{sc} values are 21.60 mA/cm², and 21.53 mA/cm^2 for TBACl and control devices, respectively. The steadystate PCE values are 19.65% and 19.18% for TBACl and control devices, respectively. The TBACl device shows more stable performance, while the control device shows a slightly declined output. The modified device could keep 99.2% of the initial PCE for 450 s, which is better than the control devices (95.3% of the initial PCE). This is related to the defect passivation in the perovskite films by TBACl. Furthermore, the current density of the control device rapidly decreases within the initial 50 s, but the modified device exhibits stable behavior, which can be seen in the inset of Fig. 4e. Fig. 4f shows the incident photon to current conversion efficiency (IPCE) spectra of the control and TBACl devices. TBACl device shows higher photoresponse intensity than the control device. It could be noticed that the peak at 620 nm shifts to 660 nm after TBACl modification. Two devices show the same thickness of the perovskite layer (Fig. 2c and d). The modified layer may influence the peak positions of the IPCE curves due to the redistribution of the optical electric field of the PSCs caused by TBACl [54,71]. Therefore, TBACl modification leads to improved electron transport, suppressed nonradiative

recombination at the interface of perovskite/ $PC_{61}BM$, and redistributed optical electric field in the devices.

UV-vis absorption spectra of the control film and the TBACl film are collected to study the influence of the TBACl on light-harvesting (Figure S11). It can be observed that the absorption curves of the TBACl and control films look identical to each other. Therefore, TBACl passivation does not influence the light-harvesting capability of perovskite films because perovskite film growth is not disturbed by the TBACl passivation due to the in-situ modification strategy, which occurs after the perovskite film growth. In addition, the PL and TRPL under the excitation of 461 nm are collected to investigate the charge recombination process influenced by TBACl. The PL intensity of TBACl film is more than 2 times higher than the control film, indicating that TBACl modifies the defects of the perovskite films effectively (Fig. 5a). Excitation light is introduced from the TBACl side (inset of Fig. 5a). TBACl blocks the excitation light to some extent, which is not considered to compare the PL intensity comparison, indicating the effective in-situ TBACl passivation. The TRPL spectra of glass/MAPbI3 and glass/ MAPbI₃/TBACl films are exhibited in Fig. 5b. MAPbI₃ modified by TBACl shows a longer lifetime compared to the control MAPbI₃. The TRPL decay curves can be fitted by the biexponential function (Eq. (2)).

$$Y = A_1 \exp\left(\frac{-t}{\tau_1}\right) + A_2 \exp\left(\frac{-t}{\tau_2}\right) \tag{2}$$

where A_1 and A_2 are the relative amplitudes. τ_1 and τ_2 are the lifetime values for the fast and slow decay processes, respectively. The fast and slow lifetime values of control MAPbI₃ film are $\tau_1=18.1$ ns and $\tau_2=18.1$ 122.1 ns, respectively. The MAPbI₃ film with TBACl displays the fast and slow lifetimes of $\tau_1=15.4$ ns and $\tau_2=193.2$ ns, respectively. The fast decay is attributed to trap-assisted non-radiative recombination at the surface [72,73], and the radiative recombination in GBs dictates the slow decay [73,74]. Therefore, the long lifetime of the modified MAPbI₃ is understood by the decreased defects and suppressed non-radiative recombination in GBs due to TBACl passivation. The time-dependent PL intensity of MAPbI₃/TBACl and MAPbI₃ films under 461 nm light excitation shows very typical light soaking effects (Fig. 5c). It is reported that defects of the perovskite films including the surface defects and GB defects will be filled by the photogenerated charge carriers under continuous light irradiation, and the rest of the electrons and holes are responsible for the PL emission [75,76]. The available photogenerated charge carriers for the PL emission increase with the decrease of defects by the photogenerated carriers under light irradiation, leading to increased PL intensity [75,76]. The PL intensity of the control film shows a fourteen-fold increase after the continuous light irradiation for 1200 s. However, a three-fold increase is obtained for the modified film, indicating reduced defects in the modified film caused by TBACl modification. Therefore, this is another evidence of the effective defect passivation by TBACl. Sub-ps-to-ns transient absorption (TA) spectroscopy measurements are carried out for the unmodified and TBAClmodified MAPbI3 films with and without the PC61BM acceptor to further understand the influence of TBACl on defect passivation and charge transport of MAPbI₃ film (Fig. 5d and e) in the fast time regime. The peak of TA spectra at \sim 760 nm is attributed to the transient photoinduced bleach [77]. The TA kinetic traces of the 760 nm bleach of the MAPbI₃/TBACl and the control film are shown in Figure \$12, which reflect the initial recombination process of charge carriers after photoexcitation [77]. The prominent slow-down of the carrier recombination process in the MAPbI₃/TBACl film compared to the unmodified sample indicates the defect passivation effect of TBACl [78]. When PC₆₁BM is present (Fig. 5f), the photoinduced bleach of MAPbI₃ first shows a ~ 10% of growth with a time constant of 25 \pm 5 ps and then rapidly decays compared to the cases without the PC₆₁BM layer. The former growth is possibly related to the contribution of the PC61BM absorption to the formation of charge carriers in the perovskite layer, while the latter decay reflects the kinetics of carrier extraction by PC61BM. The TBACl-

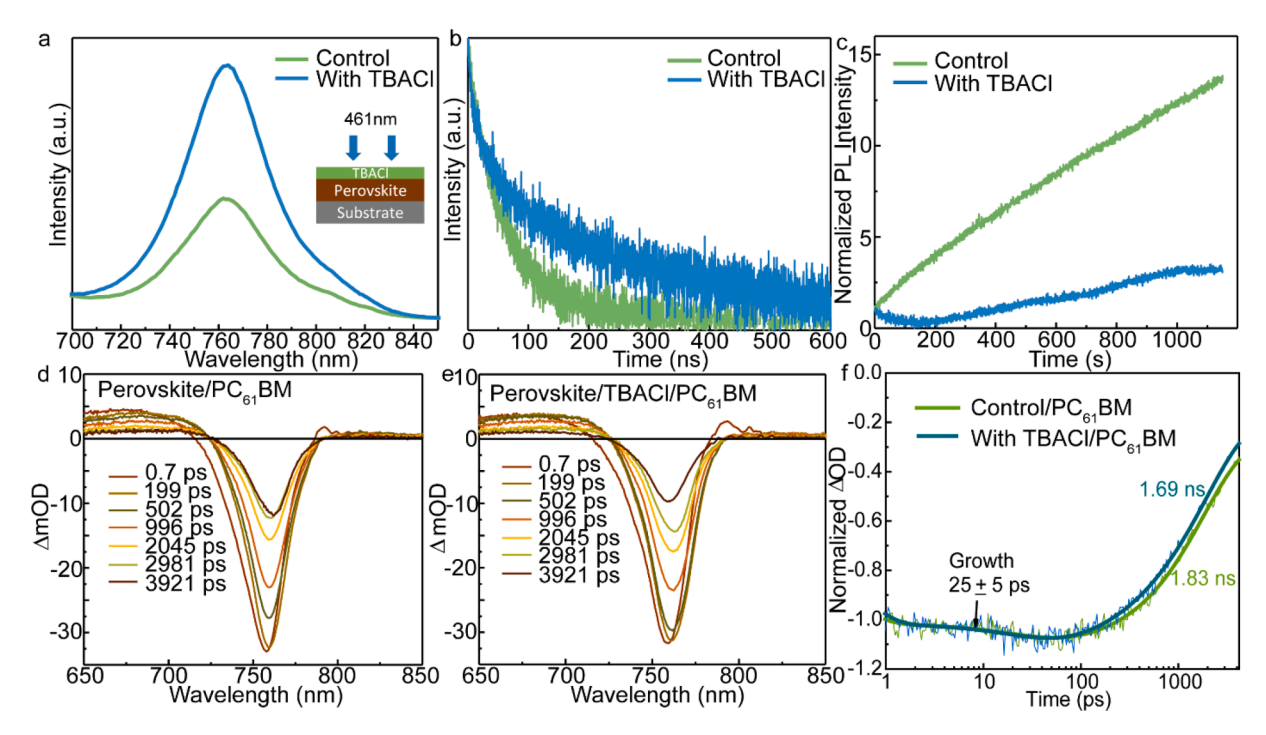


Fig. 5. The PL spectra of perovskite films with and without TBACl passivation and the structure of passivated sample for PL measurement is shown in the inset figure; b The TRPL spectra of perovskite films with and without TBACl passivation; c The normalized time-dependent PL intensity of perovskite films with and without TBACl; d-e The TA spectra of perovskite/PC61BM and perovskite/TBACl/PC61BM films; f The TA kinetics of the 760 nm bleach of perovskite/PC61BM and perovskite/TBACl/PC61BM films. Both kinetic traces are fitted with one exponential growth and one exponential decay component.

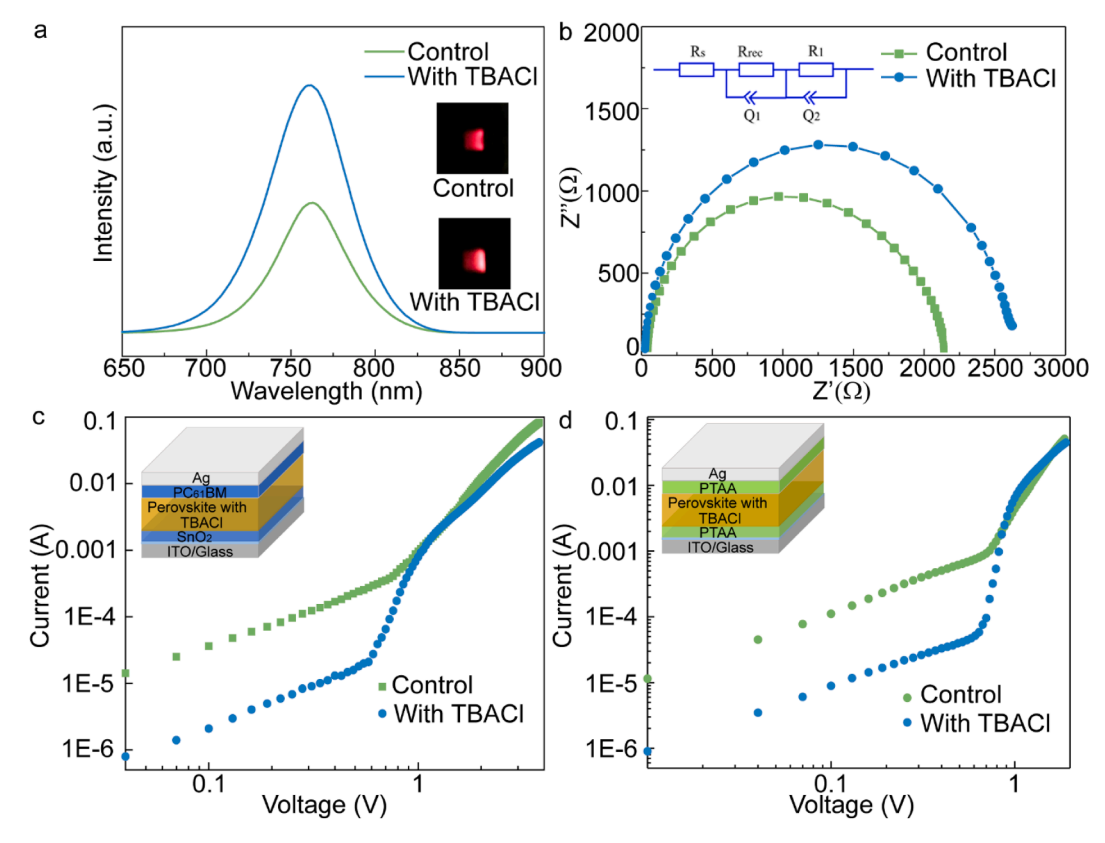


Fig. 6. a The EL spectra of the devices with and without TBACl under 1.8 V, and the photographs of the devices with and without TBACl under the bias of 1.8 V are shown in the inset; b The Nyquist plot of the PSCs with and without TBACl, and the equivalent circuit is shown in the inset; c-d The electron-only and hole-only devices with and without TBACl, the structure of devices are shown in the insets.

modified sample demonstrates a faster decay ($\tau_{1/e}=1.69\pm0.07$ ns) in contrast to the unmodified sample ($\tau_{1/e}=1.83\pm0.07$ ns), suggesting that TBACl modification can promote the charge carrier extraction process [79,80].

To study the TABCl effects on the charge recombination in the PSCs, electrochemical impedance spectra (EIS), electroluminescence (EL), and the performance of electron-only and hole-only devices are investigated for the devices with and without TABCl modification. We test EL spectra

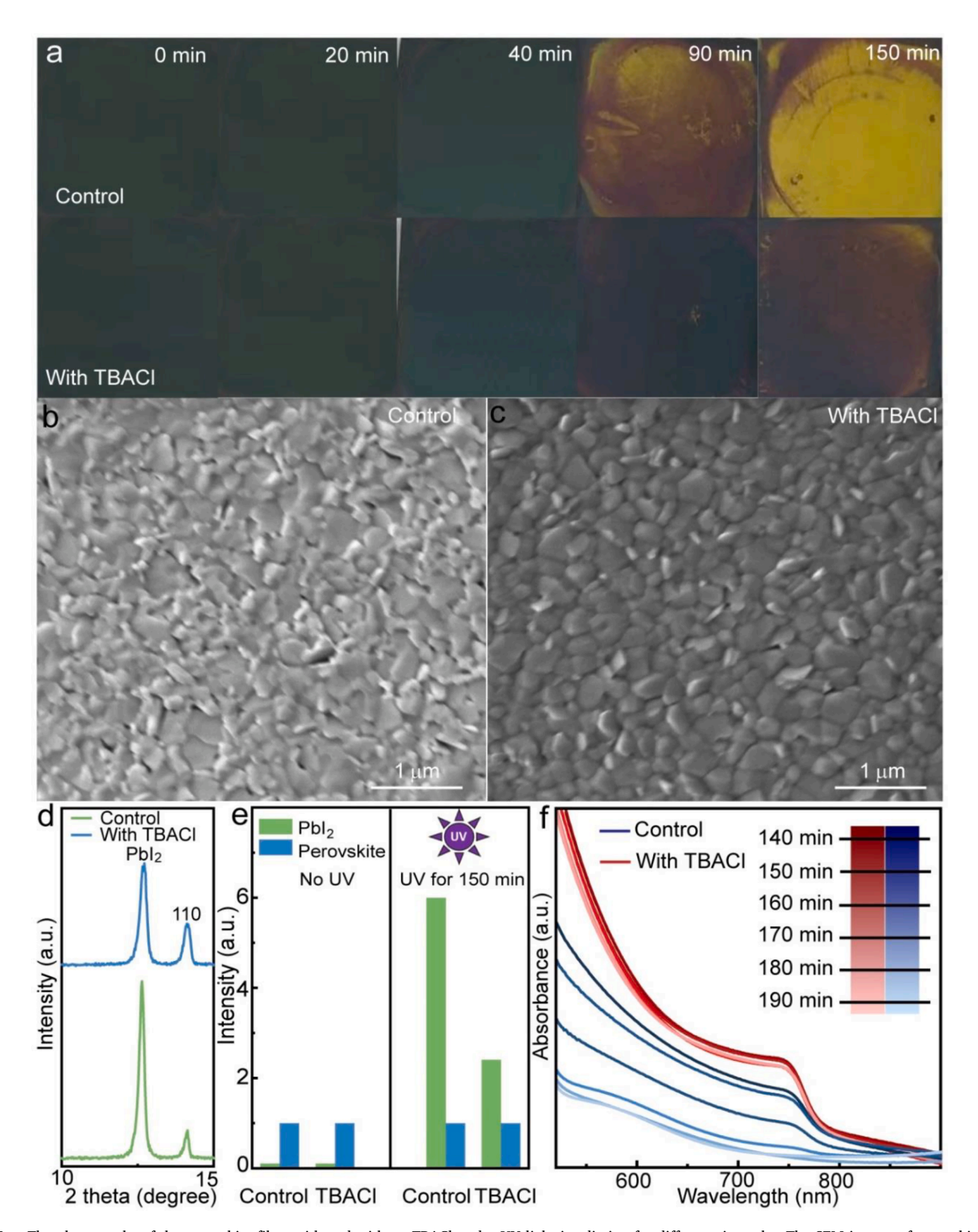


Fig. 7. a The photographs of the perovskite films with and without TBACl under UV light irradiation for different times; b-c The SEM images of perovskite film without and with TBACl under UV light irradiation for 150 min; d The XRD diffraction patterns of perovskite films with and without TBACl under UV light irradiation for 150 min; e The XRD peak intensity of perovskite and PbI₂ in the perovskite film without and with TBACl under UV light irradiation for 150 min. f The UV–vis absorption spectra of the control and TBACl films under the UV light irradiation for 140–190 min.

of PSCs with and without TBACl operating as light-emitting diode (LED) under the bias of 1.8 V (Fig. 6a). The inset shows the photographs EL of the PSCs. The PL peaks at 761 nm are observed for both devices. The PL intensity of the device with TBACl is almost twice higher than the control device, indicating the TBACl passivation reduces the defects in the devices. As shown in Fig. 6b, the Nyquist curves are obtained with 0.9 V under dark for the control and TBACl devices, and the equivalent electrical circuit model is shown in the inset of Fig. 6b [81]. The curves are well fitted with the model, and the fitting parameters are illustrated in Table S1. When the PSC is modified by TBACl, series resistance (Rs) decreases from 43.61 Ω to 23.48 Ω [74-76]. The decreased series resistance leads to increased charge transport in the devices, which may increase the device performance. The R_{rec} increases from 1805 Ω to 2544 Ω [74-76], indicating the reduced charge recombination resistance. This can reduce the charge recombination in the devices. Therefore, the charge recombination is suppressed in the devices after TBACl modification, which explains the improved FF values in J-V curves of the modified PSCs [82-84]. In addition, the electron-only and hole-only devices are fabricated to evaluate the negative and positive trap densities (Fig. 6 c and d), and the device structures are displayed in the inset of the figures. The J-V curves of electron-only and hole-only devices include three processes: The first process is the ohmic behavior $(J \propto V^1)$, then the second part is the trap-filled limit (TFL) region (J \propto Vⁿ, n \geq 3), and the final process is the space-charge limited current (SCLC) region $(J \propto V^2)$. According to the onset voltage of TFL (V_{TFL}) , the trap density could be calculated by the following equation (Eq. (3)),

$$V_{TFL} = \frac{en_t L^2}{2\varepsilon\varepsilon_0} \tag{3}$$

where V_{TFL} is the onset voltage of TFL; e is the elementary charge of an electron; L is the thickness of the perovskite film; ε and ε_0 are the relative dielectric constant of MAPbI₃ and the vacuum dielectric constant, respectively. The electron trap densities of PSCs without and with TBACl are calculated to be 4.14×10^{16} cm⁻³ and 3.74×10^{16} cm⁻³, respectively. The hole trap densities are estimated to be 4.42×10^{16} cm⁻³ for the control devices and 3.29×10^{16} cm⁻³ for the TBACl modified devices. The significantly decreased electron and hole defect densities are related to the passivation of GBs and surface defects caused by TBACl in modified devices, leading to enhanced device performance.

The stability of the PSCs including the light stability and the aging stability is another issue for the application of PSCs. The light stability of PSCs is mainly caused by the perovskite material decomposition due to UV light irradiation [85]. UV-vis absorption spectrum of TBACl in IPA is shown in Figure S13. The absorption spectrum peak of TBACl is from 260 nm to 340 nm, indicating the TBACl has strong absorption in the UV light range. Herein we carry out the UV light soaking test to study the TBACl influence on the UV light stability of PSCs. Fig. 7a exhibits photographs of the perovskite films with TBACl under continuous UV light irradiation at different time in comparison to the control films. As the UV light irradiation time is 90 min, the dominant yellow color appears for the control MAPbI₃ films, indicating the production of PbI₂ due to the decomposition of MAPbI3, while the modified film still shows dark brown color. The modified film starts to show the yellow color when the light irradiation time increases to 150 min, but the control film decomposes completely manifested by the entire yellow color. Therefore, TBACl inhibits the MAPbI₃ film degradation under UV light irradiation due to decreased defects, leading to improved UV light stability. Fig. 7b and c show the top-view SEM images of control MAPbI3 film and the TBACl film under UV light soaking for 150 min, respectively. It can be seen that the uneven grains of MAPbI3 and a lot of small particles are distributed in the GBs of the control MAPbI₃ film, while the film modified by TBACl still shows flat and even grains. This indicates the control film decomposes at the GBs[86,87]. The small particles might be PbI2 produced by the film decomposition. Figure S14 shows the SEM images of the control and modified films under different UV light

irradiation times (up to 150 min). The control film morphology changes a lot after 150 min UV light irradiation. Modified films can still maintain clear grains and uniform film morphology. These suggest the improved stability of the film by TBACl modification. In addition, the crystal structure evolution of MAPbI3 films with and without the TBACl passivation under UV light irradiation for 150 min is illustrated in Figure \$15. The intensity of PbI₂ peak at 12.66° increases with the UV light irradiation time for both films. Fig. 7d shows the XRD diffraction patterns of the control and modified films after UV light irradiation for 150 min. The relative intensity ratio of the PbI₂ (001) plane to the perovskite (110) plane ($I_{PbI2}/I_{perovskite}$) of the control film is much higher than the modified film. The normalized diffraction peak intensity ratio of PbI₂ (001) plane to perovskite (110) plane of control and TBACl films before and after UV light irradiation for 150 min are shown in Fig. 7e. The intensities are normalized by the perovskite (110) plane. The $I_{PbI2}/I_{perovskite}$ value is 0.1 for both control and modified films before UV light irradiation. The I_{PbI2}/I_{perovskite} values for the control film and the modified film increase to 6 and 2.4, respectively as the UV light irradiation time increases to 150 min. This indicates that TBACl suppresses MAPbI₃ decomposition under UV light soaking, which may be attributed to the decreased defects by TBACl passivation. Figure \$16 presents the UV-vis absorption spectra of the MAPbI₃ films with and without TBACl under UV light irradiation for different times. The modified film shows higher light absorption intensity than the control film after 150 min UV light irradiation due to the improved UV light stability, which is consistent with the results of XRD and SEM. The UV-vis absorption spectra of the films under UV light irradiation for 140–190 min are shown in Fig. 7f. It can be seen that the modified film can still keep the light-harvesting properties even under UV light irradiation for 190 min. While the UV-vis absorption features of control perovskite film disappear after UV light irradiation for 190 min. This further indicates the excellent UV light stability of the film modified by TBACl. It is considered that the degradation of perovskite starts from the GBs of perovskite films [88-90]. After TBACl passivation, TBACl modifies the GBs of the perovskite layer and decreases the defects of the films, leading to decreased rate of perovskite layer degradation. We believe this is the dominant reason for the improved stability. Another possibility is that the TABCl not only passivates the surface but also modifies the GBs of the perovskite layer. Some TBACl molecules distribute in the GBs due to the small molecule sizes, which can absorb UV light to improve the UV stability of the devices (Figure \$13).

Based on the enhanced stability of perovskite films by TBACl, we further explore the UV light stability of PSCs influenced by TBACl (Fig. 8a). The device modified by TBACl could keep over 90% of its initial PCE under continuous UV light irradiation for 450 min, and the device without TBACl only maintains \sim 51%. Thus, the UV light stability of PSCs is enhanced by TBACl passivation. The light stability of devices under continuous light irradiation without the UV component is also measured to further explore the influence of TBACl passivation on the visible light stability of the devices, as shown in Fig. 8b. The device with TBACl can maintain above 90% of the initial PCE after light soaking 120 h, but the efficiency of the control device decreases to \sim 47% of the original value. According to the previous report, the degradation of devices under light soaking leads to the production of Pb⁰ and I₂ at the interface of the perovskite/hole transport layer and perovskite/ETL [91]. TBACl could reduce I₂ to I₃ as discussed before (Fig. 1c and d). Therefore, TBACl could suppress the degradation of perovskite films under light irradiation, leading to improved light stability of PSCs. Furthermore, the PSCs are also exposed in the air (relative humidity = 30 %) without any encapsulation to evaluate the TBACl passivation effect on aging stability, which is shown in Fig. 8c. It can be seen that the PCE of the device without TBACl could maintain $\sim 39\%$ of the initial value for 30 days. Both oxygen and moisture could gradually destroy the perovskite films through defects and then cause ion migration in the devices [92]. The modified device still exhibits ~ 82% of the initial PCE after 30 days, indicating TBACl passivation suppresses the water and

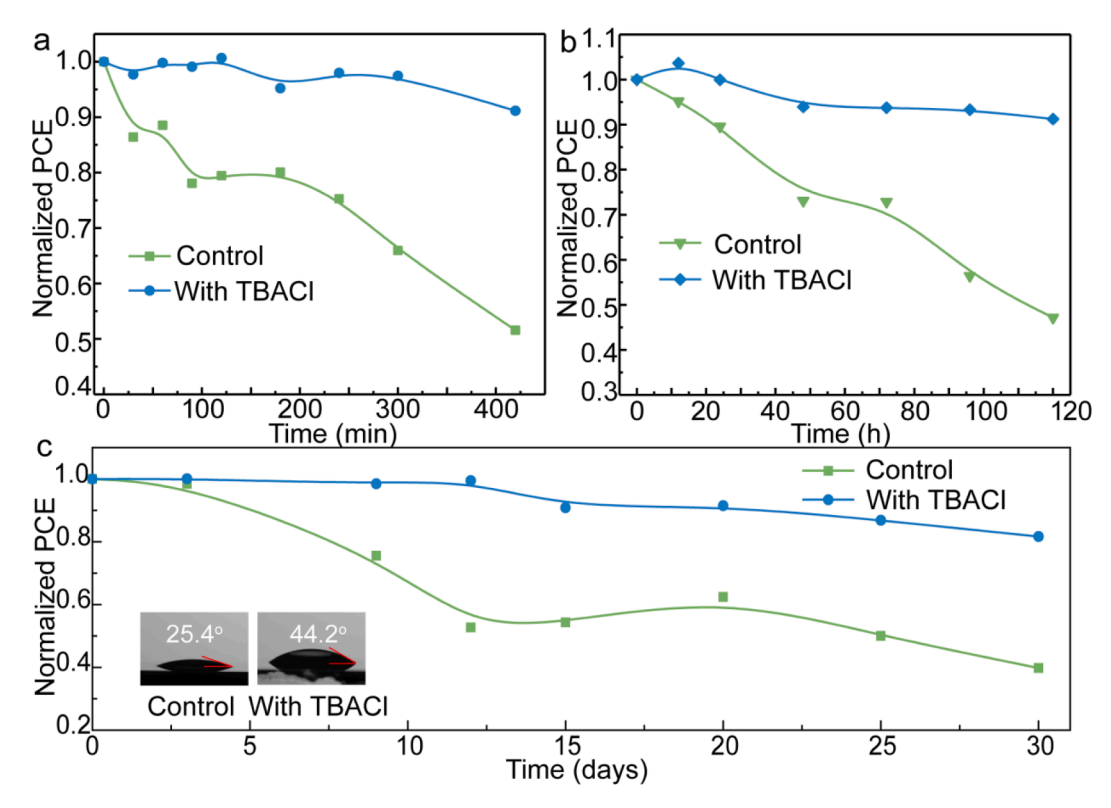


Fig. 8. a The stability of the devices with and without TBACl under UV light; b The stability of the devices with and without TBACl under a lamp; c The long-term stability of the PSCs with and without TBACl passivation in the air, and water contact photographs of perovskite films with and without TBACl are shown in the inset.

oxygen erosion to perovskite films due to the effective defect passivation. The water contact angle increases from 25.4° to 44.2° as TBACl is used to passivate the perovskite films (inset of Fig. 8c), leading to improved hydrophobic properties of the films and moisture stability of the corresponding devices by TBACl.

4. Conclusions

In this work, we demonstrate an effective method to passivate inverted PSCs in-situ. TBACl interacts with perovskite films strongly, resulting in the new phase formation. TBACl could not only passivate the surface and GB defects in situ but also modify the iodine vacancies by reducing the I2 to iodide ions to fill iodine vacancies, leading to reduced charge recombination and facilitated charge transport in the devices, which are confirmed by PL, TRPL, EL, TA, and EIS measurements. The PSCs modified by TBACl achieve PCE of 20.36%, Jsc of 23.20 mA/cm², Voc of 1.09 V, and FF of 80.52%. In addition, TBACl modification improves the stability of devices under continuous UV light irradiation and visible light soaking. The device modified by TBACl shows improved stability compared to the control device. Besides, the aging stability of the PSCs is also enhanced by TBACl passivation due to the suppressed degradation of the PSCs caused by TBACl. Therefore, the in-situ passivation by TBACl shows significant potential in optimizing the performance of PSCs toward high efficiency and high stability devices.

Declaration of Competing Interest

The authors declare that they have no known competing financial interests or personal relationships that could have appeared to influence the work reported in this paper.

Acknowledgment

This material is based on work supported by the National Science

Foundation (NSF) under Grant No. 1757220. The steady-state PL and TRPL equipment used in this work is supported by National Science Foundation Research Initiation Award: Novel Perovskite Solar Cells Based on Interface Manipulation (Award#1900047). XPS instrumentation used in this work was supported by the NSF Major Research Instrumentation Program (DMR-1726901).

Appendix A. Supplementary data

Supplementary data to this article can be found online at https://doi.org/10.1016/j.cej.2022.135647.

References

- [1] M. Kim, J. Jeong, H. Lu, T.K. Lee, F.T. Eickemeyer, Y. Liu, I.W. Choi, S.J. Choi, Y. Jo, H.-B. Kim, S.-I. Mo, Y.-K. Kim, H. Lee, N.G. An, S. Cho, W.R. Tress, S. M. Zakeeruddin, A. Hagfeldt, J.Y. Kim, M. Grätzel, D.S. Kim, Conformal quantum dot–SnO 2 layers as electron transporters for efficient perovskite solar cells, Science 375 (6578) (2022) 302–306.
- [2] D. Luo, R. Su, W. Zhang, Q. Gong, R. Zhu, Minimizing non-radiative recombination losses in perovskite solar cells, Nat. Rev. Mater. 5 (2019) 44–60, https://doi.org/ 10.1038/s41578-019-0151-y.
- [3] X. Meng, Z. Cai, Y. Zhang, X. Hu, Z. Xing, Z. Huang, Z. Huang, Y. Cui, T. Hu, M. Su, X. Liao, L. Zhang, F. Wang, Y. Song, Y. Chen, Bio-inspired vertebral design for scalable and flexible perovskite solar cells, Nat. Commun. 11 (2020), https://doi.org/10.1038/s41467-020-16831-3.
- [4] F. Li, X. Deng, F. Qi, Z. Li, D. Liu, D. Shen, M. Qin, S. Wu, F. Lin, S.-H. Jang, J. Zhang, X. Lu, D. Lei, C.-S. Lee, Z. Zhu, A.-K.-Y. Jen, Regulating Surface Termination for Efficient Inverted Perovskite Solar Cells with Greater Than 23% Efficiency, J. Am. Chem. Soc. 142 (2020) 20134–20142, https://doi.org/10.1021/iacs.0c09845.
- [5] H. Zhao, Z. Xu, Y. Che, Y. Han, S. Yang, C. Duan, J. Cui, S. Dai, Z. Liu, S. (Frank) Liu, Simultaneous dual-interface and bulk defect passivation for high-efficiency and stable CsPbI2Br perovskite solar cells, J. Power Sources. 492 (2021) 229580. https://doi.org/10.1016/j.jpowsour.2021.229580.
- [6] C. Duan, J. Cui, M. Zhang, Y. Han, S. Yang, H. Zhao, H. Bian, J. Yao, K. Zhao, Z. Liu, S. (Frank) Liu, Precursor Engineering for Ambient-Compatible Antisolvent-Free Fabrication of High-Efficiency CsPbI 2 Br Perovskite Solar Cells, Adv. Energy Mater. 10 (2020) 2000691. https://doi.org/10.1002/aenm.202000691.
- [7] Y. Han, H. Zhao, C. Duan, S. Yang, Z. Yang, Z. Liu, S. (Frank) Liu, Controlled n-Doping in Air-Stable CsPbI 2 Br Perovskite Solar Cells with a Record Efficiency of

- 16.79%, Adv. Funct. Mater. 30 (2020) 1909972. https://doi.org/10.1002/adfm.201909972.
- [8] S. Yang, J. Dai, Z. Yu, Y. Shao, Y. Zhou, X. Xiao, X.C. Zeng, J. Huang, Tailoring Passivation Molecular Structures for Extremely Small Open-Circuit Voltage Loss in Perovskite Solar Cells, J. Am. Chem. Soc. 141 (2019) 5781–5787, https://doi.org/ 10.1021/jacs.8b13091.
- [9] S. Chen, X. Xiao, H. Gu, J. Huang, Iodine reduction for reproducible and highperformance perovskite solar cells and modules, Sci. Adv. 7 (2021) 1–7, https:// doi.org/10.1126/sciadv.abe8130.
- [10] P. Calado, A.M. Telford, D. Bryant, X. Li, J. Nelson, B.C. O'Regan, P.R.F. Barnes, Evidence for ion migration in hybrid perovskite solar cells with minimal hysteresis, Nat. Commun. 7 (2016), https://doi.org/10.1038/ncomms13831.
- [11] B. Li, Y. Cai, X. Tian, X. Liang, D. Li, Z. Zhang, S. Wang, K. Guo, Z. Liu, Decorating hole transport material with –CF3 groups for highly efficient and stable perovskite solar cells, J. Energy Chem. 62 (2021) 523–531, https://doi.org/10.1016/j. iechem. 2021.04.017
- [12] W. Zhao, J. Xu, K. He, Y. Cai, Y. Han, S. Yang, S. Zhan, D. Wang, Z. Liu, S. Liu, A Special Additive Enables All Cations and Anions Passivation for Stable Perovskite Solar Cells with Efficiency over 23%, Nano-Micro Lett. 13 (2021) https://doi.org/10.1007/s40820.021.00688.2
- [13] F. Gao, Y. Zhao, X. Zhang, J. You, Recent Progresses on Defect Passivation toward Efficient Perovskite Solar Cells, Adv. Energy Mater. 10 (2019) 1902650, https://doi.org/10.1002/aenm.201902650.
- [14] F. Cai, J. Cai, L. Yang, W. Li, R.S. Gurney, H. Yi, A. Iraqi, D. Liu, T. Wang, Molecular engineering of conjugated polymers for efficient hole transport and defect passivation in perovskite solar cells, Nano Energy. 45 (2018) 28–36, https://doi.org/10.1016/j.nanoen.2017.12.028.
- [15] S. Akin, N. Arora, S.M. Zakeeruddin, M. Grätzel, R.H. Friend, M.I. Dar, New Strategies for Defect Passivation in High-Efficiency Perovskite Solar Cells, Adv. Energy Mater. 10 (2019) 1903090, https://doi.org/10.1002/aenm.201903090.
- [16] M. Wang, S. Tan, Y. Zhao, P. Zhu, Y. Yin, Y. Feng, T. Huang, J. Xue, R. Wang, G. S. Han, H.S. Jung, J. Bian, J. Lee, Y. Yang, Stable and Efficient Methylammonium-, Cesium-, and Bromide-Free Perovskite Solar Cells by In-Situ Interlayer Formation, Adv. Funct. Mater. 31 (2020) 2007520, https://doi.org/10.1002/adfm.202007520.
- [17] M. Wang, Y. Yin, W. Cai, J. Liu, Y. Han, Y. Feng, Q. Dong, Y. Wang, J. Bian, Y. Shi, Synergetic Co-Modulation of Crystallization and Co-Passivation of Defects for FAPbI 3 Perovskite Solar Cells, Adv. Funct. Mater. 32 (6) (2022) 2108567.
- [18] J. Zheng, J. Chen, D. Ouyang, Z. Huang, X. He, J. Kim, W.C.H. Choy, Critical Role of Functional Groups in Defect Passivation and Energy Band Modulation in Efficient and Stable Inverted Perovskite Solar Cells Exceeding 21% Efficiency, ACS Appl. Mater. Interfaces. 12 (2020) 57165–57173, https://doi.org/10.1021/acsami.0cl.8862
- [19] C. Luo, G. Li, L. Chen, J. Dong, M. Yu, C. Xu, Y. Yao, M. Wang, Q. Song, S. Zhang, Passivation of defects in inverted perovskite solar cells using an imidazolium-based ionic liquid, Sustain, Energy Fuels. 4 (2020) 3971–3978, https://doi.org/10.1039/ d0se00528b.
- [20] D.-Y. Son, J.-W. Lee, Y.J. Choi, I.-H. Jang, S. Lee, P.J. Yoo, H. Shin, N. Ahn, M. Choi, D. Kim, N.-G. Park, Self-formed grain boundary healing layer for highly efficient CH3NH3PbI3 perovskite solar cells, Nat. Energy. 1 (2016), https://doi. org/10.1038/nenergy.2016.81.
- [21] A. Krishna, M.A. Akhavan Kazemi, M. Sliwa, G.N.M. Reddy, L. Delevoye, O. Lafon, A. Felten, M.T. Do, S. Gottis, F. Sauvage, Defect Passivation via the Incorporation of Tetrapropylammonium Cation Leading to Stability Enhancement in Lead Halide Perovskite, Adv. Funct. Mater. 30 (2020) 1909737, https://doi.org/10.1002/ adfm.201909737.
- [22] F. Cai, Y. Yan, J. Yao, P. Wang, H. Wang, R.S. Gurney, D. Liu, T. Wang, Ionic Additive Engineering Toward High-Efficiency Perovskite Solar Cells with Reduced Grain Boundaries and Trap Density, Adv. Funct. Mater. 28 (2018) 1801985, https://doi.org/10.1002/adfm.201801985.
- [23] X. Liu, Z. Yu, T. Wang, K.L. Chiu, F. Lin, H. Gong, L. Ding, Y. Cheng, Full Defects Passivation Enables 21% Efficiency Perovskite Solar Cells Operating in Air, Adv. Energy Mater. 10 (2020) 2001958, https://doi.org/10.1002/aenm.202001958.
- [24] Z. Wu, M. Jiang, Z. Liu, A. Jamshaid, L.K. Ono, Y. Qi, Highly Efficient Perovskite Solar Cells Enabled by Multiple Ligand Passivation, Adv. Energy Mater. 10 (2020) 1903696, https://doi.org/10.1002/aenm.201903696.
- [25] S. Jin, Y. Wei, B. Rong, Y. Fang, Y. Zhao, Q. Guo, Y. Huang, L. Fan, J. Wu, Improving perovskite solar cells photovoltaic performance using tetrabutylammonium salt as additive, J. Power Sources. 450 (2020), 227623, https://doi.org/10.1016/j.jpowsour.2019.227623.
- [26] M.I. Saidaminov, J. Kim, A. Jain, R. Quintero-Bermudez, H. Tan, G. Long, F. Tan, A. Johnston, Y. Zhao, O. Voznyy, E.H. Sargent, Suppression of atomic vacancies via incorporation of isovalent small ions to increase the stability of halide perovskite solar cells in ambient air, Nat. Energy. 3 (2018) 648–654, https://doi.org/10.1038/s41560-018-0192-2.
- [27] W.-Q. Wu, P.N. Rudd, Z. Ni, C.H. Van Brackle, H. Wei, Q. Wang, B.R. Ecker, Y. Gao, J. Huang, Reducing Surface Halide Deficiency for Efficient and Stable Iodide-Based Perovskite Solar Cells, J. Am. Chem. Soc. 142 (2020) 3989–3996, https://doi.org/ 10.1021/jacs.9b13418.
- [28] N. Aristidou, C. Eames, I. Sanchez-Molina, X. Bu, J. Kosco, M.S. Islam, S.A. Haque, Fast oxygen diffusion and iodide defects mediate oxygen-induced degradation of perovskite solar cells, Nat. Commun. 8 (2017), https://doi.org/10.1038/ perpendings.
- [29] D. Barboni, R.A. De Souza, The thermodynamics and kinetics of iodine vacancies in the hybrid perovskite methylammonium lead iodide, Energy Environ. Sci. 11 (2018) 3266–3274, https://doi.org/10.1039/c8ee01697f.

- [30] F. Liu, Q. Dong, M.K. Wong, A.B. Djurišić, A. Ng, Z. Ren, Q. Shen, C. Surya, W. K. Chan, J. Wang, A.M.C. Ng, C. Liao, H. Li, K. Shih, C. Wei, H. Su, J. Dai, Is Excess Pbl2Beneficial for Perovskite Solar Cell Performance? Adv. Energy Mater. 6 (2016) 1502206, https://doi.org/10.1002/aenm.201502206.
- [31] S. Chen, X. Zhang, J. Zhao, Y. Zhang, G. Kong, Q. Li, N. Li, Y. Yu, N. Xu, J. Zhang, K. Liu, Q. Zhao, J. Cao, J. Feng, X. Li, J. Qi, D. Yu, J. Li, P. Gao, Atomic scale insights into structure instability and decomposition pathway of methylammonium lead iodide perovskite, Nat. Commun. 9 (2018), https://doi.org/10.1038/s41467-018-07177-v.
- [32] A.Y. Grishko, A.A. Eliseev, E.A. Goodilin, A.B. Tarasov, Measure is Treasure: Proper Iodine Vapor Treatment as a New Method of Morphology Improvement of Lead-Halide Perovskite Films, Chem. Mater. 32 (2020) 9140–9146, https://doi.org/ 10.1021/acs.chemmater.0c02289.
- [33] C. Shangshang, X. Xun, G. Hangyu, H. Jinsong, Iodine reduction for reproducible and high-performance perovskite solar cells and modules, Sci. Adv. 7 (2021) eabe8130, https://doi.org/10.1126/sciadv.abe8130.
- [34] Y. Ren, J. Chen, D. Ji, Y. Sun, C. Li, Improve the quality of HC(NH2)2PbIxBr 3-x through iodine vacancy filling for stable mixed perovskite solar cells, Chem. Eng. J. 384 (2020), 123273, https://doi.org/10.1016/j.cej.2019.123273.
- [35] Y. Du, J. Wu, X. Zhang, Q. Zhu, M. Zhang, X. Liu, Y. Zou, S. Wang, W. Sun, Surface passivation using pyridinium iodide for highly efficient planar perovskite solar cells, J. Energy Chem. 52 (2021) 84–91, https://doi.org/10.1016/j. iechem.2020.04.049.
- [36] X. Bu, R.J.E. Westbrook, L. Lanzetta, D. Ding, T. Chotchuangchutchaval, N. Aristidou, S.A. Haque, Surface Passivation of Perovskite Films via Iodide Salt Coatings for Enhanced Stability of Organic Lead Halide Perovskite Solar Cells, Sol. RRL. 3 (2018) 1800282, https://doi.org/10.1002/solr.201800282.
- [37] X. Jiang, S. Chen, Y. Li, L. Zhang, N. Shen, G. Zhang, J. Du, N. Fu, B. Xu, Direct Surface Passivation of Perovskite Film by 4-Fluorophenethylammonium Iodide toward Stable and Efficient Perovskite Solar Cells, ACS Appl. Mater. Interfaces. 13 (2021) 2558–2565, https://doi.org/10.1021/acsami.0c17773.
- [38] N.H. Tiep, Z. Ku, H.J. Fan, Recent Advances in Improving the Stability of Perovskite Solar Cells, Adv. Energy Mater. 6 (2015) 1501420, https://doi.org/ 10.1002/aenm.201501420.
- [39] S. Ito, S. Tanaka, K. Manabe, H. Nishino, Effects of Surface Blocking Layer of Sb2S3 on Nanocrystalline TiO2 for CH3NH3PbI3 Perovskite Solar Cells, J. Phys. Chem. C. 118 (2014) 16995–17000, https://doi.org/10.1021/jp500449z.
- [40] K. Deng, Q. Chen, Y. Shen, L. Li, Improving UV stability of perovskite solar cells without sacrificing efficiency through light trapping regulated spectral modification, Sci. Bull. 66 (23) (2021) 2362–2368.
- [41] F. Bella, G. Griffini, J.-P. Correa-Baena, G. Saracco, M. Grätzel, A. Hagfeldt, S. Turri, C. Gerbaldi, Improving efficiency and stability of perovskite solar cells with photocurable fluoropolymers, Science 354 (6309) (2016) 203–206.
- [42] H. Zheng, G. Liu, L. Zhu, J. Ye, X. Zhang, A. Alsaedi, T. Hayat, X. Pan, S. Dai, Enhanced Performance and Stability of Perovskite Solar Cells Using NH4I Interfacial Modifier, ACS Appl. Mater. Interfaces. 9 (2017) 41006–41013, https://doi.org/10.1021/acsami.7b12721.
- [43] S.-W. Lee, S. Kim, S. Bae, K. Cho, T. Chung, J.-K. Hwang, I. Song, W. Lee, S. Park, J. Jung, J. Chun, Y.J. Lee, Y.J. Moon, H.-S. Lee, D. Kim, C. Bin Mo, Y. Kang, Enhanced UV stability of perovskite solar cells with a SrO interlayer, Org. Electron. 63 (2018) 343–348, https://doi.org/10.1016/j.orgel.2018.09.019.
- [44] W.S. Yang, B.-W. Park, E.H. Jung, N.J. Jeon, Y.C. Kim, D.U. Lee, S.S. Shin, J. Seo, E. K. Kim, J.H. Noh, S.I. Seok, Iodide management in formamidinium-lead-halide-based perovskite layers for efficient solar cells, Science 356 (6345) (2017) 1376–1379.
- [45] C. Shangshang, X. Xun, G. Hangyu, H. Jinsong, Iodine reduction for reproducible and high-performance perovskite solar cells and modules, Sci. Adv. 7 (2022) eabe8130, https://doi.org/10.1126/sciadv.abe8130.
- [46] Q. Sun, X. Gong, H. Li, S. Liu, X. Zhao, Y. Shen, M. Wang, Direct formation of I3ions in organic cation solution for efficient perovskite solar cells, Sol. Energy Mater. Sol. Cells. 185 (2018) 111–116, https://doi.org/10.1016/j. solmat 2018 05 017
- [47] G. Tumen-Ulzii, C. Qin, D. Klotz, M.R. Leyden, P. Wang, M. Auffray, T. Fujihara, T. Matsushima, J. Lee, S. Lee, Y. Yang, C. Adachi, Detrimental Effect of Unreacted PbI 2 on the Long-Term Stability of Perovskite Solar Cells, Adv. Mater. 32 (2020) 1905035, https://doi.org/10.1002/adma.201905035.
- [48] T.J. Jacobsson, J.-P. Correa-Baena, E. Halvani Anaraki, B. Philippe, S.D. Stranks, M.E.F. Bouduban, W. Tress, K. Schenk, J. Teuscher, J.-E. Moser, H. Rensmo, A. Hagfeldt, Unreacted PbI2 as a Double-Edged Sword for Enhancing the Performance of Perovskite Solar Cells, J. Am. Chem. Soc. 138 (2016) 10331–10343, https://doi.org/10.1021/jacs.6b06320.
- [49] A.A. Sutanto, N. Drigo, V.I.E. Queloz, I. Garcia-Benito, A.R. Kirmani, L.J. Richter, P.A. Schouwink, K.T. Cho, S. Paek, M.K. Nazeeruddin, G. Grancini, Dynamical evolution of the 2D/3D interface: a hidden driver behind perovskite solar cell instability, J. Mater. Chem. A. 8 (2020) 2343–2348, https://doi.org/10.1039/ c9ta12480f
- [50] W. Kim, M.S. Jung, S. Lee, Y.J. Choi, J.K. Kim, S.U. Chai, W. Kim, D.-G. Choi, H. Ahn, J.H. Cho, D. Choi, H. Shin, D. Kim, J.H. Park, Oriented Grains with Preferred Low-Angle Grain Boundaries in Halide Perovskite Films by Pressure-Induced Crystallization, Adv. Energy Mater. 8 (2017) 1702369, https://doi.org/ 10.1002/aenm.201702369.
- [51] C. Lu, Z. Hu, Y. Wang, K. Sun, B. Shen, C. Gao, C. Yang, J. Zhang, Y. Zhu, Carrier Transfer Behaviors at Perovskite/Contact Layer Heterojunctions in Perovskite Solar Cells, Adv. Mater. Interfaces. 6 (2018) 1801253, https://doi.org/10.1002/ admi.201801253.

- [52] S. Mabrouk, B. Bahrami, A. Gurung, K.M. Reza, N. Adhikari, A. Dubey, R. Pathak, S. Yang, Q. Qiao, Higher efficiency perovskite solar cells using additives of LiI, LiTFSI and BMImI in the PbI2 precursor, Sustain, Energy Fuels. 1 (2017) 2162–2171, https://doi.org/10.1039/c7se00435d.
- [53] W. Yang, R. Su, D. Luo, Q. Hu, F. Zhang, Z. Xu, Z. Wang, J. Tang, Z. Lv, X. Yang, Y. Tu, W. Zhang, H. Zhong, Q. Gong, T.P. Russell, R. Zhu, Surface modification induced by perovskite quantum dots for triple-cation perovskite solar cells, Nano Energy. 67 (2020), 104189, https://doi.org/10.1016/j.nanoen.2019.104189.
- [54] J. Xiong, Z. Dai, S. Zhan, X. Zhang, X. Xue, W. Liu, Z. Zhang, Y. Huang, Q. Dai, J. Zhang, Multifunctional passivation strategy based on tetraoctylammonium bromide for efficient inverted perovskite solar cells, Nano Energy. 84 (2021), 105882, https://doi.org/10.1016/j.nanoen.2021.105882.
- [55] T. Glaser, C. Müller, M. Sendner, C. Krekeler, O.E. Semonin, T.D. Hull, O. Yaffe, J. S. Owen, W. Kowalsky, A. Pucci, R. Lovrinčić, Infrared Spectroscopic Study of Vibrational Modes in Methylammonium Lead Halide Perovskites, J. Phys. Chem. Lett. 6 (2015) 2913–2918, https://doi.org/10.1021/acs.jpclett.5b01309.
- [56] Y. Wang, T. Mahmoudi, W.-Y. Rho, H.-Y. Yang, S. Seo, K.S. Bhat, R. Ahmad, Y.-B. Hahn, Ambient-air-solution-processed efficient and highly stable perovskite solar cells based on CH3NH3Pbi3-xClx-NiO composite with Al2O3/NiO interfacial engineering, Nano Energy. 40 (2017) 408–417, https://doi.org/10.1016/j.
- [57] B. Ma, J. Chen, M. Wang, X. Xu, J. Qian, Y. Lu, W. Zhang, P. Xia, M. Qin, W. Zhu, L. Zhang, S. Chen, X. Lu, W. Huang, Passivating Charged Defects with 1,6-Hexamethylenediamine To Realize Efficient and Stable Tin-Based Perovskite Solar Cells, J. Phys. Chem. C. 124 (2020) 16289–16299, https://doi.org/10.1021/acs.ipcc.0r03401.
- [58] Z. Zhang, J. Liang, Y. Zheng, X. Wu, J. Wang, Y. Huang, Y. Yang, Z. Zhou, L. Wang, L. Kong, K.M. Reddy, C. Qin, C.-C. Chen, Balancing crystallization rate in a mixed Sn-Pb perovskite film for efficient and stable perovskite solar cells of more than 20% efficiency, J. Mater. Chem. A. 9 (2021) 17830–17840, https://doi.org/10.1039/dlta04922d
- [59] H. Kim, J.W. Lee, G.R. Han, S.K. Kim, J.H. Oh, Synergistic Effects of Cation and Anion in an Ionic Imidazolium Tetrafluoroborate Additive for Improving the Efficiency and Stability of Half-Mixed Pb-Sn Perovskite Solar Cells, Adv. Funct. Mater. 31 (2020) 2008801, https://doi.org/10.1002/adfm.202008801.
- [60] S.-W. Kim, G. Kim, C.s. Moon, T.-Y. Yang, J. Seo, Metal-Free Phthalocyanine as a Hole Transporting Material and a Surface Passivator for Efficient and Stable Perovskite Solar Cells, Small, Methods, 5 (5) (2021) 2001248.
- [61] M. Saliba, L. Etgar, Current Density Mismatch in Perovskite Solar Cells, ACS Energy Lett. 5 (2020) 2886–2888, https://doi.org/10.1021/acsenergylett.0c01642.
- [62] A.A. Sutanto, P. Caprioglio, N. Drigo, Y.J. Hofstetter, I. Garcia-Benito, V.I. E. Queloz, D. Neher, M.K. Nazeeruddin, M. Stolterfoht, Y. Vaynzof, G. Grancini, 2D/3D perovskite engineering eliminates interfacial recombination losses in hybrid perovskite solar cells, Chem. 7 (2021) 1903–1916, https://doi.org/10.1016/j. chempr.2021.04.002.
- [63] J. Haddad, B. Krogmeier, B. Klingebiel, L. Krückemeier, S. Melhem, Z. Liu, J. Hüpkes, S. Mathur, T. Kirchartz, Analyzing Interface Recombination in Lead-Halide Perovskite Solar Cells with Organic and Inorganic Hole-Transport Layers, Adv. Mater. Interfaces. 7 (2020) 2000366, https://doi.org/10.1002/ admi/202000366
- [64] J.H. Noh, S.H. Im, J.H. Heo, T.N. Mandal, S., Il Seok, Chemical Management for Colorful, Efficient, and Stable Inorganic-Organic Hybrid Nanostructured Solar Cells, Nano Lett. 13 (2013) 1764–1769, https://doi.org/10.1021/nl400349b.
- [65] Y.H. Khattak, F. Baig, A. Shuja, L. Atourki, K. Riaz, B.M. Soucase, Device Optimization of PIN Structured Perovskite Solar Cells: Impact of Design Variants, ACS Appl. Electron. Mater. 3 (2021) 3509–3520, https://doi.org/10.1021/ acsaelm.1c00460.
- [66] S. Ryu, J.H. Noh, N.J. Jeon, Y. Chan Kim, W.S. Yang, J. Seo, S., Il Seok, Voltage output of efficient perovskite solar cells with high open-circuit voltage and fill factor, Energy Environ. Sci. 7 (2014) 2614–2618, https://doi.org/10.1039/ c4ee00762i.
- [67] S.N. Habisreutinger, N.K. Noel, H.J. Snaith, Hysteresis Index: A Figure without Merit for Quantifying Hysteresis in Perovskite Solar Cells, ACS Energy Lett. 3 (2018) 2472–2476, https://doi.org/10.1021/acsenergylett.8b01627.
- [68] D.-H. Kang, N.-G. Park, On the Current-Voltage Hysteresis in Perovskite Solar Cells: Dependence on Perovskite Composition and Methods to Remove Hysteresis, Adv. Mater. 31 (2019) 1805214, https://doi.org/10.1002/adma.201805214.
- [69] M. Wang, W. Li, H. Wang, K. Yang, X. Hu, K. Sun, S. Lu, Z. Zang, Small Molecule Modulator at the Interface for Efficient Perovskite Solar Cells with High Short-Circuit Current Density and Hysteresis Free, Adv. Electron. Mater. 6 (2020) 2000604, https://doi.org/10.1002/aelm.202000604.
- [70] W. Li, D. Wang, W. Hou, R. Li, W. Sun, J. Wu, Z. Lan, High-Efficiency, Low-Hysteresis Planar Perovskite Solar Cells by Inserting the NaBr Interlayer, ACS Appl. Mater. Interfaces. 13 (2021) 20251–20259, https://doi.org/10.1021/ acsami.1c04806.
- [71] J. Gilot, I. Barbu, M.M. Wienk, R.A.J. Janssen, The use of ZnO as optical spacer in polymer solar cells: Theoretical and experimental study, Appl. Phys. Lett. 91 (11) (2007) 113520.
- [72] B. Liu, H. Bi, D. He, L. Bai, W. Wang, H. Yuan, Q. Song, P. Su, Z. Zang, T. Zhou, J. Chen, Interfacial Defect Passivation and Stress Release via Multi-Active-Site Ligand Anchoring Enables Efficient and Stable Methylammonium-Free Perovskite

- Solar Cells, ACS Energy Lett. 6 (2021) 2526–2538, https://doi.org/10.1021/acsenergylett.1c00794.
- [73] P. Guo, Q. Ye, X. Yang, J. Zhang, F. Xu, D. Shchukin, B. Wei, H. Wang, Surface & grain boundary co-passivation by fluorocarbon based bifunctional molecules for perovskite solar cells with efficiency over 21%, J. Mater. Chem. A. 7 (2019) 2497–2506, https://doi.org/10.1039/C8TA11524A.
- [74] T. Handa, D.M. Tex, A. Shimazaki, A. Wakamiya, Y. Kanemitsu, Charge Injection Mechanism at Heterointerfaces in CH3NH3PbI3 Perovskite Solar Cells Revealed by Simultaneous Time-Resolved Photoluminescence and Photocurrent Measurements, J. Phys. Chem. Lett. 8 (2017) 954–960, https://doi.org/10.1021/acs. ipclett.6b02847.
- [75] C. Zhao, B. Chen, X. Qiao, L. Luan, K. Lu, B. Hu, Revealing Underlying Processes Involved in Light Soaking Effects and Hysteresis Phenomena in Perovskite Solar Cells, Adv. Energy Mater. 5 (2015) 1500279, https://doi.org/10.1002/ aemy 201500279
- [76] S. Shao, M. Abdu-Aguye, T.S. Sherkar, H.-H. Fang, S. Adjokatse, G. ten Brink, B. J. Kooi, L.J.A. Koster, M.A. Loi, The Effect of the Microstructure on Trap-Assisted Recombination and Light Soaking Phenomenon in Hybrid Perovskite Solar Cells, Adv. Funct. Mater. 26 (2016) 8094–8102, https://doi.org/10.1002/adfm 201602519
- [77] L. Wang, C. McCleese, A. Kovalsky, Y. Zhao, C. Burda, Femtosecond Time-Resolved Transient Absorption Spectroscopy of CH3NH3Pbl3 Perovskite Films: Evidence for Passivation Effect of Pbl2, J. Am. Chem. Soc. 136 (2014) 12205–12208, https://doi.org/10.1021/ja504632z.
- [78] M. Zhou, J.S. Sarmiento, C. Fei, H. Wang, Charge Transfer and Diffusion at the Perovskite/PCBM Interface Probed by Transient Absorption and Reflection, J. Phys. Chem. C. 123 (2019) 22095–22103, https://doi.org/10.1021/acs. ipcc.9b07591.
- [79] E. Ugur, J.I. Khan, E. Aydin, M. Wang, M. Kirkus, M. Neophytou, I. McCulloch, S. De Wolf, F. Laquai, Carrier Extraction from Perovskite to Polymeric Charge Transport Layers Probed by Ultrafast Transient Absorption Spectroscopy, J. Phys. Chem. Lett. 10 (2019) 6921–6928, https://doi.org/10.1021/acs.jpclett.9b02502.
- [80] E. Serpetzoglou, I. Konidakis, G. Kakavelakis, T. Maksudov, E. Kymakis, E. Stratakis, Improved Carrier Transport in Perovskite Solar Cells Probed by Femtosecond Transient Absorption Spectroscopy, ACS Appl. Mater. Interfaces. 9 (2017) 43910–43919. https://doi.org/10.1021/acsami.7b15195.
- [81] Z. Hu, J.M. García-Martín, Y. Li, L. Billot, B. Sun, F. Fresno, A. García-Martín, M. U. González, L. Aigouy, Z. Chen, TiO2 Nanocolumn Arrays for More Efficient and Stable Perovskite Solar Cells, ACS Appl. Mater. Interfaces. 12 (2020) 5979–5989, https://doi.org/10.1021/acsami.9b21628.
- [82] Q. Lou, G. Lou, R. Peng, Z. Liu, W. Wang, M. Ji, C. Chen, X. Zhang, C. Liu, Z. Ge, Synergistic Effect of Lewis Base Polymers and Graphene in Enhancing the Efficiency of Perovskite Solar Cells, ACS Appl. Energy Mater. 4 (2021) 3928–3936, https://doi.org/10.1021/acsaem_1c00299.
- [83] C. Mai, Q. Zhou, Q. Xiong, C. Chen, J. Xu, Z. Zhang, H. Lee, C. Yeh, P. Gao, Donor-A-Acceptor Type Porphyrin Derivatives Assisted Defect Passivation for Efficient Hybrid Perovskite Solar Cells, Adv. Funct. Mater. 31 (2020) 2007762, https://doi.org/10.1002/adfm.202007762.
- [84] Y. Cai, J. Cui, M. Chen, M. Zhang, Y. Han, F. Qian, H. Zhao, S. Yang, Z. Yang, H. Bian, T. Wang, K. Guo, M. Cai, S. Dai, Z. Liu, S. (Frank) Liu, Multifunctional Enhancement for Highly Stable and Efficient Perovskite Solar Cells, Adv. Funct. Mater. 31 (2020) 2005776. https://doi.org/10.1002/adfm.202005776.
- [85] N.N. Shlenskaya, N.A. Belich, M. Grätzel, E.A. Goodilin, A.B. Tarasov, Light-induced reactivity of gold and hybrid perovskite as a new possible degradation mechanism in perovskite solar cells, J. Mater. Chem. A. 6 (2018) 1780–1786, https://doi.org/10.1039/c7ta10217h.
- [86] Y. Hui, Y. Tan, L. Chen, Z. Nan, J. Zhou, J. Yan, B. Mao, Stability of Perovskite Thin Films under Working Condition: Bias-Dependent Degradation and Grain Boundary Effects, Adv. Funct. Mater. 31 (2021) 2103894, https://doi.org/10.1002/ adfp. 202103894
- [87] X. Ma, L. Yang, X. Shang, M. Li, D. Gao, C. Wu, S. Zheng, B. Zhang, J. Chen, C. Chen, H. Song, Grain boundary defect passivation by in situ formed wide-bandgap lead sulfate for efficient and stable perovskite solar cells, Chem. Eng. J. 426 (2021) 130695. https://doi.org/10.1016/j.csi.2021.120695.
- 426 (2021), 130685, https://doi.org/10.1016/j.cej.2021.130685.
 [88] Q. Wang, B. Chen, Y. Liu, Y. Deng, Y. Bai, Q. Dong, J. Huang, Scaling behavior of moisture-induced grain degradation in polycrystalline hybrid perovskite thin films, Energy Environ. Sci. 10 (2017) 516–522, https://doi.org/10.1039/c6ee02941h.
- [89] Z. Wang, A. Pradhan, M.A. kamarudin, M. Pandey, S.S. Pandey, P. Zhang, C.H. Ng, A.S.M. Tripathi, T. Ma, S. Hayase, Passivation of Grain Boundary by Squaraine Zwitterions for Defect Passivation and Efficient Perovskite Solar Cells, ACS Appl, Mater. Interfaces. 11 (10) (2019) 10012–10020.
- [90] N. Phung, A. Abate, The Impact of Nano- and Microstructure on the Stability of Perovskite Solar Cells, Small. 14 (2018) 1802573, https://doi.org/10.1002/ smll 201802573
- [91] T. Sekimoto, T. Matsui, T. Nishihara, R. Uchida, T. Sekiguchi, T. Negami, Influence of a Hole-Transport Layer on Light-Induced Degradation of Mixed Organic-Inorganic Halide Perovskite Solar Cells, ACS Appl. Energy Mater. 2 (2019) 5039–5049, https://doi.org/10.1021/acsaem.9b00709.
- [92] M.I. Asghar, J. Zhang, H. Wang, P.D. Lund, Device stability of perovskite solar cells – A review, Renew. Sustain. Energy Rev. 77 (2017) 131–146, https://doi.org/ 10.1016/j.rser.2017.04.003.